Diverse Structures and Dimensionalities in Zn(II), Cd(II), and Hg(II) Metal Complexes with Piperonylic Acid

Daniel Ejarque,[†] Francisco Sánchez-Férez,[†] JoséA. Ayllón,[†] Teresa Calvet,[‡] MercèFont-Bardia,[§] and Josefina Pons[*,†]

† Departament de Química, Universitat Autònoma de Barcelona, 08193-Bellaterra, Barcelona, Spain
‡ Cristal·lografia, Mineralogia I Dipòsits Minerals, Universitat de Barcelona, Martí i Franquès s/n, 08028 Barcelona, Spain
§ Unitat de Difraccióde Raig-X, Centres Científics i Tecnològics de la Universitat de Barcelona (CCiYUB), Universitat de Barcelona, Solé i Sabarís, 1-3, 08028 Barcelona, Spain

Josefina.Pons@uab.es..(J. Pons))

ORCID

Daniel Ejarque: 0000-0002-1014-1128

Francisco Sánchez-Férez: 0000-0002-9546-6828

José A. Ayllón: 0000-0001-7965-7424

Teresa Calvet: 0000-0002-4058-7171

Mercè Font-Bardia: 0000-0002-7892-8744

Josefina Pons: 0000-0003-1834-9326

ABSTRACT:

Reaction of M(MeCO2)2 (M = Zn(II), Cd(II), and Hg(II)) with 1,3-benzodioxole-5-carboxylic acid (HPip) in methanol (MeOH) yields four piperonylate compounds, one of Zn(II) ([Zn(Pip)2(H2O)2] (1c)), two of Cd(II) ([Cd(μ-Pip)2(H2O)]n (2) and [Cd3(μ-Pip)6(MeOH)2]n (3)), and one of Hg(II) ([Hg(μ- Pip)2]n (4)). The obtention of compounds 1c and 4 was independent of the M/L ratio. These four compounds were characterized by analytical and spectroscopic techniques. In addition, the thermal stability of 1c, 2, and 4 has been studied, and the structure of all the complexes has been determined by the single crystal X-ray diffraction method. The Zn(II) compound displayed a monomeric structure, while Cd(II) and Hg(II) complexes exhibited three polymeric arrays. The Zn(II) (1c) and Hg(II) (4) centers are four- and eight-coordinated in a tetrahedral or squareantiprism geometry, respectively. Furthermore, the Cd(II) ions are either six- (2) or six- and seven- (3) coordinated in a octahedral or both octahedral and pentagonal bipyramid geometries, respectively. In these compounds, the Pip ligand presents different coordination modes: μ1-η1 (1c); μ2-η1:η1 and μ2-η2:η1 (2); μ2-η1:η1, μ2-η2:η1 and μ3-η2:η1:η1 (3); μ1-η2 and μ2-η2:η1 (4). The extended structures were also analyzed. Their photoluminescence properties have been examined, and the quantum yields have been calculated.

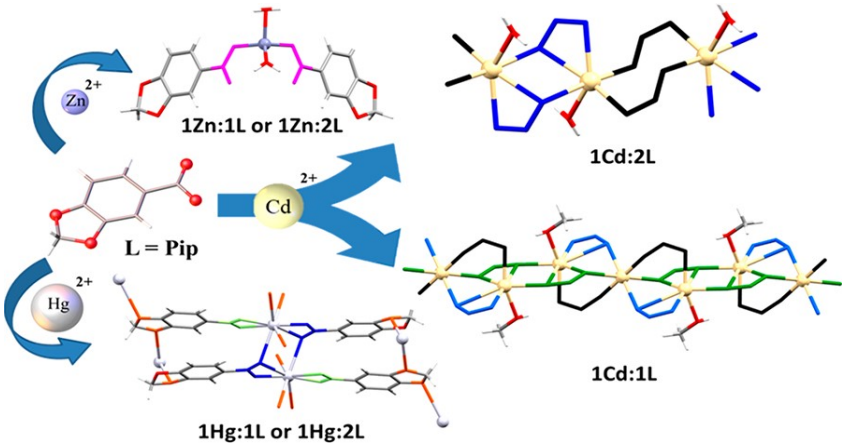

INTRODUCTION

The design of one-, two-, or three-dimensional frameworks by a ligand to metal approach represents one of the most promising modern research areas.1−3 The formation of these nets is based on the assembly of metal nodes and organic linkers through coordination bonds resulting in the named coordination polymers (CPs). CPs have attracted great interest in the past two decades for their versatile structures, their diverse topologies,4 and therefore, their potential applications in gas storage,5 energy storage,6 host−guest chemistry,7 catalysis,8 or luminescence.9

There are many factors that dictate the final structural disposition: the ionic counterions, the noncovalent forces, the metal/linker ratio, the temperature, or the solvent polarity. Zn(II), Cd(II), and Hg(II) as metal d10 ions contribute to eliminate the ligand field effects favoring the generation of diverse geometries. Between them, Cd(II) and Hg(II) centers have a larger ionic radius that allows flexibility in coordination numbers.

It is noteworthy that Zn(II) and Cd(II) CPs gained much interest for their ability to form bonds and their extraordinary physical properties.10,11 Regarding Hg(II) CPs, few reported compounds containing aromatic carboxylates have been reported. Their huge van der Waals radius (1.50 Å) allows the inclusion of many atoms in the coordination sphere, but only those comprised below the sum of their van der Waals radii must be considered as coordinated atoms.12 This structural feature produces low solubility complexes and dense packed structures.13,14

Many efforts have been devoted to the modification of this kind of architecture to achieve novel properties, but all these fore-mentioned factors must be controlled. Any slight modification causes a structural change, thus, in their properties.15 Puong et al. verified this assertion with the synthesis of Zn(II), Cd(II), and Hg(II) dioxole containing carboxylates which generated different structures and properties in comparison with those previously performed without the dioxole unit.16 In this case, the coordination of the dioxole unit to the metal centers contributes to the final scaffold. All of these reactions were performed in solvothermal conditions. There are not many previously reportd CPs with carboxylate linkers incorporating a dioxole group which participates through coordination bonds in the structural inception.

The 1,3-benzodioxole-5-carboxylic acid (piperonylic acid, HPip) is a benzoic acid derivative and a versatile ligand, which could present a great variety of coordination modes also involving the dioxole group. Our group has been studying its structural behavior during the last few years in combination with pyridine derivative ligands. Most of these complexes were formed using the Cu(MeCO2)2·H2O salt and provided monomeric and dimeric arrays. Among a total of 16 complexes, eight are paddle-wheel,17−20 two are dimeric arrays,17,21 and six have a monomeric structure.17,18 The coordination modes present in these cases were monodentate, bidentate chelate, and syn-syn bidentate bridged. In one of them, the HPip unit was occluded instead of coordinated.21 The use of Pip and pyridine derivatives with d10 metal ions (Zn(II), Cd(II), and Hg(II)) generated four dimeric compounds, two of them paddle-wheels

and two dimeric. In this case, the Pip units displayed a bidentate chelate and a bidentate bridged coordination mode.22 In this contribution, trying to better understand the behaviour of the Pip ligand, we have performed its reactions against M(MeCO2)2 (M = Zn(II), Cd(II), and Hg(II)) in mild conditions. The structural versatility of the Pip ligands in combination with the variety of geometries provided by the metal centers has generated four complexes with diverse geometries and topologies. The Zn(II) metal probably as a result of its smaller radius has formed a monomeric specie with labile coordinated ammonia units, which rapidly exchanges with water from the solvent resulting in the compound [Zn(Pip)2(H2O)2] (1c). Besides that, the bigger Cd(II) and Hg(II) radius together with the mentioned versatility of the Pip ligand promoted the formation of three coordination polymers [Cd(μ-Pip)2(H2O)]n (2), [Cd3(μ-Pip)6(MeOH)2]n (3), and [Hg(μ-Pip)2]n (4). It is noteworthy the coordination of the dioxole oxygen atoms in the polymeric Hg(II) structure which underpin the 3D structural formation (Scheme 1).

EXPERIMENTAL SECTION

Materials and General Methods. Zinc(II) acetate dehydrate (Zn(MeCO2)2·2H2O), cadmium(II) acetate dihydrate (Cd- (MeCO2)2·2H2O), mercury(II) acetate (Hg(MeCO2)2), 1,3-benzodioxole-5-carboxylic acid (piperonylic acid, HPip) ligand, ammonia solution (NH3) and methanol (MeOH) as solvent were purchased from Sigma-Aldrich and used without further purification. All the reactions and manipulations were carried out in air at room temperature (r.t.) except for compound [Cd3(μ-Pip)6(MeOH)2]n (3), which was carried out under reflux conditions. Elemental analyses (C, H, N) were carried on a Euro Vector 3100 instrument. HR-ESI-MS measurements were recorded after dissolving the corresponding solid complexes in MeOH for 1c, 2, and 4 and DMSO/MeOH (2 mL:8 mL) for 3 in a MicroTOF-Q (Bruker Daltonics GmbH, Bremen, Germany) instrument equipped with an electrospray ionization source (ESI) in positive mode. Na+ ions comes from the MeOH solvent which contains <50 ppb. Conditions were those used in routine experiments. The nebulizer pressure was 1.5 bar, the desolvation temperature was 180 °C, dry gas at 6 L min−1, the capillary counter-electrode voltage was 5 kV, and the quadrupole ion energy, 5.0 eV. FTIR-ATR spectra were recorded on a Tensor 27 (Bruker) spectrometer, equipped with an attenuated total reflectance (ATR) accessory model MKII Golden Gate with diamond window in the range 4000−500 cm−1. 1H NMR spectra were recorded on an NMR-FT Bruker400 MHz spectrometer in DMSO-d6 solution at r.t. 13C{1H} NMR spectra of compounds [Zn(Pip)2(H2O)2] (1c), [Cd(Pip)2(H2O)]n (2), and [Hg(Pip)2]n (4) and DEPT-135 NMR spectra of compound 2 were recorded on an NMR-FT Bruker360 MHz spectrometer in DMSO-d6 solution at r.t. All chemical shifts (δ) are given in ppm relative to TMS as an internal standard. Simultaneous TG/DTA determinations were carried out in a Netzsch STA 409 instrument, with an aluminum oxide powder (Al2O3) crucible and heating at 5 °C·min−1 from 25 to 380 °C, under a nitrogen atmosphere with a flow rate of 80 mL·min−1. Al2 O3 (PerkinElmer 0419-0197) was used as a standard. The electronic spectra in solution of MeOH (≈1.25 × 10−5 M) were run on a Agilent HP 8453 UV−vis spectrophotometer with a quartz cell having path length of 1 cm in the range of 190−350 nm. Fluorescence measurements were carried out with a PerkinElmer LS 55 50 Hz fluorescence spectrometer using 1 cm quartz cell, in methanol solution. The emission spectra were measured at 25 °C. The samples were excited at 291 nm, and the emission were recorded between 305 and 500 nm. The data obtained were corrected for the dilution effects by means of the Origin Pro 8 software.

Synthesis of [Zn(Pip)2(NH3)2] (1a). A MeOH solution (20 mL) of Zn(MeCO2)2·2H2O (151 mg, 0.688 mmol) was added dropwise to a solution (30 mL) of HPip (115 mg, 0.689 mmol) with NH3 (0.5 mL, 8.36 mmol) in MeOH as solvent at r.t. The resulting colorless solution was stirred for 24 h, filtered, and kept in the fridge. After 10 min, a minimum quantity of crystalline powder was obtained. 1H NMR (400 MHz; DMSO-d6; Me4Si; 298 K): δ = 7.54 [2H, dd, 3J = 8.1 Hz, 4J = 1.6 Hz, O2C−CH−CH], 7.38 [2H, d, 4J = 1.5 Hz, O2C−CH−CO], 6.90 [2H, d, 3J = 8.1 Hz, O2C−CH−CH], 6.06 [4H, s,O−CH2−O], 3.11 [6H, s, NH3].

Synthesis of [Zn(Pip)2(H2O)(NH3)] (1b). A MeOH solution (20 mL) of Zn(MeCO2)2·2H2O (151 mg, 0.689 mmol) was added dropwise to a solution (30 mL) of HPip (115 mg, 0.689 mmol) with NH3 (0.5 mL, 8.36 mmol) in MeOH as solvent at r.t. The resulting colorless solution was stirred for 24 h, filtered, and kept in the fridge. Yellowish crystals were obtained after 1 day. Unfortunately, its crystal structure could not be elucidated. Yield: 21.0 mg (7.09%) (respect to Zn(MeCO2)2·2H2O). Elemental analysis calc (%) for C16H15NO9Zn (430.68) C 44.62; H 3.51; N 3.25; found: C 44.45; H 3.37; N 3.01%. FTIR-ATR (wavenumber, cm−1): 3355−3317(br) [ν(O−H)water], 3270−3177(br) [ν(N−H)ammonia], 3073(w) [ν(C−H)ar], 2999−2790(br) [ν(C−H)al], 1628(w) [νas(CO2)], 1575(m), 1498(w), 1483(w), 1433(s) [νs(CO2)], 1374(m), 1345(s), 1250(s), 1235(s), 1163(m) [ν(C−O−C)], 1112(m), 1073(w), 1038(s) [δip(C−H)], 936(m), 916(s), 844(w), 820(w), 805(s), 779(s) [δoop(C−H)], 722(m), 663(s), 580(s). 1H NMR (400 MHz; DMSO-d6; Me4Si; 298 K): δ = 7.51 [2H, dd, 3J = 8.1 Hz, 4J = 1.6 Hz, O2C−CH−CH], 7.35 [2H, d, 4J = 1.5 Hz, O2C−CH−CO], 6.87 [2H, d, 3J = 8.1 Hz, O2C−CH−CH], 6.03 [4H, s, O−CH2−O], 3.13 [3H, s, NH3].

Synthesis of [Zn(Pip)2(H2O)2] (1c). A MeOH solution (20 mL) of Zn(MeCO2)2·2H2O (151 mg, 0.688 mmol) was added dropwise to a solution (30 mL) of HPip (114 mg, 0.688 mmol) with NH3 (0.5 mL, 8.36 mmol) in MeOH as solvent at r.t. The resulting colorless solution was stirred for 24 h, filtered, and kept in the fridge. After 6 days, suitable colorless crystals were obtained. The resulting crystals were filtered off and washed with cold MeOH (5 mL) and dried under a vacuum. Yield: 79.7 mg (27%) (respect to Zn(MeCO2)2· 2H2O). Elemental analysis calc(%) for C16H14O10Zn (431.67): C 44.52; H 3.27; found: C 44.31; H 3.12%. HR-MS (ESI+, MeOH): m/z (%) = 416.9613 (100%) (calc. for [Zn(Pip)2 + Na]+ = 416.9559). FTIR-ATR (wavenumber, cm−1): 3342(m) [ν(O−H)water], 3245(w), 3173−3007(br) [ν(C−H)ar], 2931−2850(br) [ν(C−H)al], 1628(w) [vas(CO2)], 1590(m), 1500(w), 1478(w), 1432(s) [νs(CO2)], 1335(s), 1253(s), 1236(s), 1164(m) [ν(C−O−C)], 1114(w), 1103(w), 1075(w), 1036(s) [δip(C−H)], 933(w), 918(m), 903(m), 839(w), 820(w), 805(m), 779(s) [δoop(C−H)], 681(w), 661(s), 611(w), 585(m). 1H NMR (400 MHz; DMSO-d6; Me4Si; 298 K): δ = 7.53 [2H, dd, 3J = 8.1 Hz, 4J = 1.6 Hz, O2C−CH−CH], 7.37 [2H, d, 4J = 1.6 Hz, O2C−CH−CO], 6.89 [2H, d, 3J = 8.1 Hz, O2C−CH−CH], 6.05 [4H, s, O−CH2−O]. 13C{1H} NMR (360 MHz; DMSOd6; Me4Si; 298 K): δ = 171.62 [O2C−C−CH−CH], 149.31 [O2C−C−CH−CH−C], 146.81 [O2C−C−CH−C], 129.50 [O2C−C−CH−CH], 124.54 [O2C−C−CH−C], 109.51 [O2C−C−CH−C], 107.44 [O2C−C−CH−CH−C], 101.33 [O−CH2−O]. UV−vis: (MeOH, 9.96 × 10−8 M) λmax = 206 nm; 254 nm; 292 nm.

Synthesis of [Cd(μ-Pip)2(H2O)]n (2). A MeOH solution (10 mL) of Cd(MeCO2)2·2H2O (156 mg, 0.585 mmol) was added dropwise to a solution (18 mL) of HPip (195 mg, 1.17 mmol) with NH3 (0.5 mL, 8.36 mmol) in MeOH as solvent at r.t. The resulting solution was stirred for 2 h until a white solid precipitated. The powder was filtered and dried under a vacuum. Suitable colorless crystals were obtained by recrystallization in MeOH for 3 days. Yield: 131 mg (49%) (respect to Cd(MeCO2)2·2H2O). Elemental analysis calc(%) for C16H12CdO9 (460.67): C 41.72; H 2.63; found: C 41.49; H 2.57%.HR-MS (ESI+, MeOH): m/z (%) = 902.8681 (18%) (calc. for [Cd2(Pip)4 + Na]+ =

902.8721; 730.9115 (10%) (calc. for [Cd2(Pip)3(H2O)]+ = 730.8755); 712.9111 (11%) (calc. for [Cd2(Pip)3]+ = 712.8650); 440.9476 (38%) (calc. for [Cd(Pip)2 +H]+ = 440.9478). FTIR-ATR (wavenumber, cm−1): 3416−3258(sh) [ν(O−H)water], 3133−3034(br) [ν(C−H)ar], 2997−2777(br) [ν(C−H)al], 1655(w), 1630(w), 1606(w) [νas(CO2)], 1548(m) [νas(CO2)], 1503(s), 1487(s), 1437(s) [νs(CO2)], 1384(s), 1348(s), 1260(s), 1240(s), 1167(m) [ν(C−O−C)], 1111(s), 1077(w), 1034(s) [δip(C−H)], 934(m), 922(s), 885(m), 830(w), 806(m), 775(s) [δoop(C−H)], 722(m), 680(m). 1H NMR (400 MHz; DMSO-d6; Me4Si; 298 K): δ = 7.54 [2H, d, 3J = 8.1 Hz, O2C−CH−CH], 7.39 [2H, s, O2C−CH−CO], 6.92 [2H, d, 3J = 8.2 Hz, O2C−CH−CH], 6.07 [4H, s, O−CH2−O]. 13C{1H} NMR (360 MHz; DMSO-d6; Me4Si; 298 K): δ = 171.62 [O2C−C−CH−CH], 149.31 [O2C−C−CH−CH−C], 146.81 [O2C−C−CH−C], 129.50 [O2C−C−CH−CH], 124.54 [O2C−C−CH−C], 109.51 [O2C−C−CH−C], 107.44 [O2C−C−CH−CH−C], 101.33 [O−CH2−O]. DEPT-135 NMR(360 MHz; DMSO-d6; Me4Si; 298 K): δ = 124.54 [O2C−C−CH−C], 109.51 [O2C−C−CH−C], 107.44 [O2C−C−CH−CH−C], 101.33 [O−CH2−O]. (UV−vis: (MeOH, 1.02 × 10−7 M) λmax = 216 nm; 255 nm; 292 nm.

Synthesis of [Cd3(μ-Pip)6(MeOH)2]n (3). A MeOH solution (20 mL) of Cd(MeCO2)2·2H2O (150 mg, 0.563 mmol) was added dropwise to a solution (30 mL) of HPip (93.7 mg, 0.564 mmol) with NH3 (0.5 mL, 8.36 mmol) in MeOH as solvent under reflux conditions and stirred for 10 h. The solution was concentrated under a vacuum and kept in the fridge during 4 days until crystals were obtained. Suitable colorless crystals were obtained by recrystallization in MeOH and keeping the solution in the fridge during a few hours. Yield: 81.9 mg (31%) (respect to Cd(MeCO2)2·2H2O). Elemental analysis calc(%) for C50H38Cd3O26 (1392.05): C 43.14; H 2.75; found: C 42.98; H 2.54. HR-MS (ESI+, DMSO/MeOH): m/z (%) = 352.9346 (42%) (calc. for [Cd(Pip)(DMSO)]+ = 352.9352). FTIRATR (wavenumber, cm−1): 3611(m) [ν(O−H)MeOH], 3074(w) [ν(C−H)ar], 2996(w), 2933−2703(br) [ν(C−H)al], 2663(w), 2604(w), 1627(w) [νas(CO2)], 1562(s) [νas(CO2)], 1500(m), 1492(m) [νs(CO2)], 1435(s) [νs(CO2)], 1375(s), 1345(s), 1251(s), 1162(m) [ν(C−O−C)], 1108(m), 1071(m), 1041(s) [δip(C−H)], 932(m), 916(s), 800(m), 769(s) [δoop(C−H)], 717(s), 704(s), 676(s). 1H NMR (400 MHz; DMSO-d6; Me4 Si; 298 K): δ = 7.54 [6H, dd, 3J = 8.1 Hz, 4J = 1.6 Hz, O2C−CH−CH], 7.38 [6H, d, 4J = 1.4 Hz, O2C−CH−CO], 6.91 [6H, d, 3J = 8.1 Hz, O2C−CH−CH], 6.06 [12H, s, O−CH2−O]. UV−vis: (MeOH, 9.98 × 10−8 M) λmax = 214 nm; 255 nm; 292 nm.

Synthesis of [Hg(μ-Pip)2]n (4). A MeOH solution (15 mL) of Hg(MeCO2)2 (225 mg, 0.707 mmol) was added dropwise to a solution (35 mL) of HPip (235 mg, 1.42 mmol) in MeOH as solvent at r.t. and stirred for 1 h and a half until a white solid precipitated. The resulting white solid was filtered, and the mother liquors were evaporated under a vacuum. Suitable colorless crystals were obtained by slow evaporation of mother liquors in air for 12 days. Yield: 308 mg (82%) (respect to Hg(MeCO2)2). Elemental analysis calc(%) for C16H10HgO8 (530.83): C 36.20; H 1.90; found: C 35.98; H 1.74. HRMS (ESI+, MeOH): m/z (%) = 1079.9968 (17%) (calc. for [Hg2(Pip)4+Na]+ = 1079.9996); 550.9919 (30%) (calc. for [Hg-(Pip)2+Na]+ = 550.9936); 507.0044 (31%) (calc. for [Hg(Pip)2 −CO2 +

Na]+ = 507.0037). FTIR-ATR (wavenumber, cm−1): 3115−3010(br) [ν(C−H)ar], 2990−2905(br) [ν(C−H)al], 1633(m) [vas(CO2)], 1619(m), 1602(m), 1565(m) [vas(CO2)], 1504(m), 1485(s) [νs(CO2)], 1437(s) [νs(CO2)], 1403(w), 1370(s), 1329(m), 1295(s), 1240(s), 1158(s) [ν(C−O−C)], 1108(s), 1072(m), 1034(s) [δ(C−H)ip], 1025(s) [δ(C−H)ip], 943(w), 930(m), 921(s), 910(s), 894(s), 887(s), 837(w), 823(m), 808(s), 756(s) [δ(C−H)oop], 723(s) [δ(C−H)oop], 719(s) [δ(C−H)oop], 692(s), 671(m), 610(m), 593(m), 574(m), 562(m), 551 (m). 1H NMR (400 MHz; DMSO-d6; Me4Si; 298 K): δ = 7.58 [2H, dd, 3J = 8.1 Hz, 4J = 1.6 Hz, O2C−CH−CH], 7.40 [2H, d, 4J = 1.6 Hz, O2C−CH-CO], 7.00 [2H, d, 3J = 8.1 Hz, O2C−CH−CH], 6.12 [4H, s, O−CH2−O]. 13C{1H} NMR (360 MHz; DMSO-d6; Me4Si; 298 K): δ = 168.90 [O2C−C−CH−CH], 150.33 [O2C−C−CH−CH−C], 147.22 [O2C−C−CH−C], 125.14 [O2C−C-CH−CH; O2C−C−CH−C], 109.48 [O2C−C−CH−C], 107.92 [O2C−C−CH−CH−C], 101.75 [O−CH2−O]. UV−vis: (MeOH, 9.95 × 10−8 M) λmax = 214 nm; 256 nm; 293 nm.

X-ray Crystallographic Data. For compounds 1c and 4, a colorless plate-like while for 2 and 3, colorless prism-like specimens were used for the X-ray crystallographic analysis. The X-ray intensity data were measured on a D8 Venture system equipped with a multilayer monochromate and a Mo microfocus (λ = 0.71073 Å). For 1c−4, the frames were integrated with the Bruker SAINT Software package using a narrow-frame algorithm.

The structures were solved using the Bruker SHELXTL Software, package and refined using SHELX (version-2018/3).23 For 1c−4, the final cell constants and volume, are based upon the refinement of the XYZ-centroids of reflections above 20 σ(I). Data were corrected for absorption effects using the multiscan method (SADABS). Crystal data and relevant details of structure refinement for compounds 1c−4 are reported in Table 1 and in the Supporting Information. Complete information about the crystal structure and molecular geometry is available in CIF format deposited with the CCDC. CCDC 1938412 (1c), 1938411 (2), 1938414 (3), and 1938413 (4) contain the supplementary data for this paper. Molecular graphics were generated with the program Mercury 3.624,25 with POV-Ray package26 and Olex2 software.27 Color codes for all molecular graphics: blue (Zn), yellow (Cd), light gray (Hg), red (O), dark gray (C), and white (H).

RESULTS AND DISCUSSION

Syntheses and Characterization. Compounds 1c−4were prepared via combination of HPip and M(MeCO2)2 (M = Zn(II), Cd(II), Hg(II)) salts in MeOH as solvent at r.t. except for 3, which has been performed under reflux. It must be noted that during the reaction between the Zn(II) salt and the HPip ligand, three different Zn(II) complexes have been identified (1a−1c).

Single crystals for X-ray crystallographic analysis were grown at low temperature (4 °C) for 1c, recrystallization in MeOH for compounds 2 (in air) and 3 (at low temperature, 4 °C), and slow evaporation of mother liquors for 4.

Reaction between M(MeCO2)2·xH2O (M = Zn(II) and Hg(II)) and HPip ligand yielded compounds 1c and 4 regardless of the M/Pip ratio (1:1 or 1:2). In contrast, the synthesis starting from Cd(MeCO2)2 resulted in two different complexes depending on the M/Pip ratio; the 1:1 proportion yielded 3, while the 1:2 proportion formed complex 2. Compound 1a was characterized by 1H NMR spectroscopy while 1b by elemental analysis, FTIR-ATR and 1H NMR spectroscopies. Unfortunately, crystals of 1b were not suitable for structural determination. Compounds 1c−4 were characterized by HR-ESI-MS, elemental analysis, FTIR-ATR, 1H, 13C{1H}, and DEPT-135 NMR spectroscopies and single crystal X-ray diffraction method. The thermal stability of compounds 1c, 2, and 4 was studied via TG/DTA determinations. Finally, the UV−vis and fluorescence properties of compounds 1c−4 were analyzed and their quantum yields were calculated.

The elemental analyses of compounds 1b−4 agree with the proposed formula. The positive ionization mass spectra (ESI+-MS) of all the compounds were recorded using MeOH (1c, 2, and 4) or MeOH/DMSO (3) as solvent. In this condition, 3 is broken, resulting in small fragments as m/z 352.9346 (42%) [Cd(Pip)(DMSO)]+ (S.I: Figure S1). Compound 1c shows a peak at m/z 416.9613 (100%) attributable to [1c − 2H2O +Na]+ (S.I: Figure S2), in which the water molecules are lost during the ESI fragmentation. Compound 4 showed the peak at m/z 1079.9968 (17%) attributable to [Hg2(Pip)4 + Na]+(S.I: Figure S3a). Additional fragments have been identified at m/z 550.9919 (30%), corresponding to the monomeric unit [Hg(Pip)2 + Na]+ (S.I: Figure S3b) and at m/z 507.0044 (31%), to the decarboxylation product [Hg(Pip)2-CO2 + Na]+(S.I: Figure S3c). For 2, the peaks at m/z 440.9476 (38%) and m/z 902.8681 (18%) have been assigned to the monomeric [Cd(Pip)2 + H]+ and dimeric [Cd2(Pip)4+Na]+ units without the coordinated water molecule, respectively (S.I: Figure S4). Other fragments, which suggest the polymeric array is maintained in solution, have been found at m/z 712.9111 (11%) and at m/z 730.9115 (10%) and assigned to [Cd2(Pip)3]+ and [Cd2(Pip)3(H2O)]+, respectively (Figure 1).

The FTIR-ATR spectra of compounds 1b and 1c display the characteristic carboxylate bands at 1628 cm−1 for νas(CO2) and 1433−1432 cm−1 for νs(CO2). The difference between these bands [Δ = νas(CO2) − νs(CO2)]28,29 is 195 and 196 cm−1 for compounds 1b and 1c, respectively, suggesting a monodentate coordination mode of the carboxylate ligands (S.I: Figures S5 and S6). Besides,

compounds 2−4 exhibit values between 111 and 128 cm−1, which indicate a bidentate chelate coordination mode of the carboxylate groups. Moreover, compounds 2−4 present additional Δ values in the range 135−169 cm−1, indicating the presence of different bridging coordination modes (S.I: Figures S7−S9). The bands attributable to the aromatic groups [ν(C⨁C)], [δ(C−H)ip], and [δ(C−H)oop] are also identified.30

The presence of solvent molecules allows further identification of some specific bands. Compounds 1c, 1b, and 2 present peaks attributable to ν(O−H)water in the range of 3416−3258 cm−1, while in compound 1b the peaks assigned to ν(N−H)ammonia appear between 3270 and 3177 cm−1. Compound 3 presents a sharp peak at 3611 cm−1 attributable to ν(O−H)MeOH. Therefore, the FTIR-ATR spectra data agree with the structures determined by the single crystal X-ray diffraction method.

NMR Experiments. 1H NMR spectra of complexes 1a−4 as well as 13C{1H} NMR of complexes 1c, 2, and 4 have been recorded in DMSO-d6. Unfortunately, 3 was not soluble enough in DMSO-d6 and in common solvents for the 13C{1H} NMR experiment. In the 1H NMR spectra of compounds 1a−4, the signals attributable to the aromatic protons appeared between 7.58 and 6.87 ppm and the aliphatic protons of the dioxole unit between 6.12 and 6.03 ppm (HPip: 7.54−7.00 and 6.12). The 1H NMR spectra confirm the coordination of the Pip ligand to the metal center (S.I: Figures S10−S13). In compounds 1a−1c, the NMR experiments were carried out for studying the NH3−H2O exchange by the decrease of the signal at 3.1 ppm corresponding to the protons of NH3 molecules, which indicates the time dependent exchange of two NH3 molecules by two H2O molecules (S.I: Figure S10). The first 1H NMR probe was done from the small quantity of crystallization product of 1a in DMSO-d6 solution at time zero (t0) (S.I: Figure 10a). The same solution was exposed to air for 24 h (t1). The 1H NMR measurement of this aerated sample (S.I: Figure 10b) denoted a change in the intensity and shape of the ammonia peak present at 3.1 ppm, and for this reason an additional measurement of the same sample was performed after 6 days (t2 = 7 days). In this case, the ammonia signal disappeared (S.I: Figure 10c). Likewise, the intensity of the water signal at 3.36 increased inversely proportional to the ammonia because DMSO is an hygroscopic solvent.

In the 13C{1H} NMR spectra of complexes 1c, 2, and 4, the signals of the carbons of the carboxylate groups appeared between 171.62 and 168.90 ppm followed by the aromatic carbons between 150.33 and 107.44 ppm. Finally, the aliphatic carbon of the dioxole unit appeared between 101.75 and 101.33 ppm (HPip: 166.69, 151.19−108.12, and 101.99 ppm) (S.I: Figures S14−S16). DEPT-135 spectrum of 2 has been recorded to confirm the assignation of C2 and C3 atoms (S.I: Figure S15b). The displacement of the peak assigned to C1 atom suggests the coordination of the carboxylate group to the corresponding metal centers. Further NMR data are provided in the Experimental Section.

Coordination Modes of the Carboxylate. Owing to the diverse structures presented by the Pip ligand, we listed its most common coordination modes highlighting those present in this work for clarification (Scheme 2).

Structural Description of [Zn(Pip)2(H2O)2] (1c). The crystalline powder of compounds 1a−1c was obtained from the same reaction using Zn(MeCO2)2·2H2O, HPip, and NH3 with MeOH as solvent. From this reaction, only single crystals of compound 1c could be grown for the single crystal X-ray diffraction method.

Compound 1c belongs to the orthorhombic Pna21 space group and contains two crystallographically independent molecules in the unit cell, with similar bond lengths and angles (molecules A and B) (Table 2). Both have the same monomeric structure with a [ZnO4] core, composed by two μ1-η1 Pip units and two H2O molecules (Figure 2). The Zn(II) center displays a slightly distorted tetrahedral geometry with bond angles ranging from 102.5(3) to 120.7(3)° for molecule A and from 101.7(3) to 120.0(3)° for molecule B (Table 2).

In both molecules, the monodentate H2O molecules present slightly longer Zn−Owater distances (A, 1.992(6)−2.044(6) Å; B, 1.998(6)−2.055(6) Å) in comparison with those belonging from the Zn−OPip bonds (A, 1.975(7)−1.979(6) Å; B, 1.973(6)−1.977(6) Å for Zn−Owater). The values of distances and angles are similar to other reported tetrahedral Zn(II) complexes with the same [ZnO4] core also having two oxygen atoms belonging from H2O molecules and two oxygen atoms from carboxylate moieties ([Zn(sul)2(H2O)2] (sul = sulindac, C20H17FO3S),31 [Zn(2,4-D)2(H2O)2] (2,4-D = 2,4-dichlorophenoxyacetic acid)32 or [Zn(C11H7O3)2(H2O)2] (C11H7O3 = 3-hydroxynaphthalene-2-carboxylate)33).

The coordinated water molecules present in A and B exhibit different supramolecular behaviors. The two water molecules belonging to the B molecule participate in the formation of the nets through the two hydrogen atoms, while in the A molecule, only one water molecule participates with the two hydrogens and the remaining water molecule participates with only one hydrogen atom. These molecules A and B are joined via two hydrogen bond interactions. The two protons of the coordinated H2O molecule of B, with the shorter bond distance, exhibit two moderate hydrogen bond interactions34 with the two uncoordinated carboxylate oxygen atoms of A (O9B−H9C···O2A, 2.27(7); O9B−H9D···O6A, 2.31(7) Å) forming a supramolecular dimeric unit (Figure 3a).

These supramolecular dimeric units are held together by four moderate hydrogen bond interactions. Two of them are promoted by the water molecule with shorter bond distance of A, which interacts with two uncoordinated carboxylate oxygen atoms of two different monomers, one from A (O9A−H9A··· O2A, 2.41(6)Å) and one from B (O9A−H9B···O2B, 2.37(7) Å)). The other two interactions are driven by the remaining water molecule of B with the two coordinated carboxylate oxygen atoms of another B molecule (O10B−H10D···O5B, 2.32(9); O10B−H10C···O1B, 2.45(9) Å). All these set of interactions expand the structure forming 1D chains along the b axis (Figure 3b). It could be noted that in B the μ1-η1 coordination mode of the carboxylate moiety is probably driven by the supramolecular interactions with the water molecules (O9A−H9B···O2B and O10B−H10D···O5B).

In addition, the water molecule of A, which only participates with one hydrogen bond, interacts with a coordinated carboxylate oxygen atom of B expanding the structure along the a axis

(O10A−H10A···O1B, 2.51(9) Å) together with the interactions from the supramolecular dimeric units (Figure 4a). Finally, B molecules of different chains are joined via a C−H···π interaction between the Pip aromatic ring and one aliphatic proton of the dioxole moiety through the c axis (Figure 4b) supported by the interactions of the supramolecular dimeric units, which display a 3D net (Figure 5) (Table 3).

Structural Description of [Cd(Pip)2(H2O)]n (2). This compound belongs to the monoclinic C2/c space group. It consists in a polymeric 1D chain with each Cd(II) ions presenting a [CdO6] core. This core is composed by five carboxylate oxygen atoms from four Pip ligands and a water molecule, which display an hexacoordinated compound. The distortion on the geometry is evaluated through the average twist angle.35,36 While higher average twist angles around 60° belongs from octahedral geometry, the lower values close to 0° pertain to a trigonal prism geometry. Compound 2 exhibits an average twist angle of 58.62° (O6−Cg3−Cg4−O5, 56.01°; O9−Cg3−Cg4−O2#2, 73.07°; O2−Cg3−C4−O1, 46.77°) indicating a distorted octahedral geometry with Cd−O bond distances in the range of 2.200(7) to 2.393(7) Å (Figure 6a; Table 4). The Cd−O bond distances are similar to other structures with Cd(II) metal centers and carboxylate ligands.37 Cd(II) ions are connected in an alternate manner due to the presence of two different coordination modes of the Pip ligands. Two bridging Pip units link one pair of Cd(II) via μ2-η2:η1, while the other two Pip units link these Cd(II) centers with the contiguous Cd(II) ions via μ2-η1:η1. These pairs of equally coordinated Cd(II) ions present a 2-fold axis inversion center, which expands through the ab direction along the 1D polymeric chain (Figure 6b).

In this octahedral geometry, the equatorial positions are occupied by four oxygen atoms situated in the base of the octahedron corresponding to the Pip ligands, which presents two different types of bridging coordination modes, O5 and O6 atoms adopts the μ2-η1:η mode while O2 and O2(#1) the μ2-η2:η1 mode. The oxygen atoms of the water molecules and the ones of the ligand with μ2-η2:η coordination, which have the shorter bond distance (O1), are located at the apical positions. The presence of the μ2-η2:η1coordination mode seems to produce the distortion of the octahedral geometry due to the displacement of the ditopic carboxylate oxygen atoms respect to the axial plane of the octahedron (O9−Cd1−O1, 136.6(3)). This alternate coordination mode also sets two different consecutive distances (Cd(1)···Cd(1) (3.705(1) Å) and Cd(1)···Cd(1) (4.382(1) Å)). The close packing of the structure allows the formation of intramolecular π−π interactions between the phenyl rings of the Pip ligands (Cg1···Cg2, 3.852(3)). (Table 4).

The coordinated water molecules promote two hydrogen bond interactions along the b axis. One with the η1 oxygen atoms of the Pip units presents the μ2-η2:η1 coordination mode, which has the longer distance to the metal center (Cd1−O1, 2.371(7) Å), and the other with the oxygen atoms with shorter bond distance (Cd1−O1, 2.314(6) Å) to the Pip units with the μ2-η1:η1 coordination mode (Figure 7a). The weaker intermolecular forces are the C−H···O interactions along the c axis, which are formed between one oxygen atom of the dioxole rings with one aliphatic proton of the another dioxole ring of the Pip ligand. All these sets of interactions expand the structure forming a 3D net (Figure 7b).

Structural Description of [Cd3(Pip)6(MeOH)2]n (3). This compound belongs to the monoclinic P21/n space group. Its crystal structure consists of a polymeric 1D chain with two crystallographically independent Cd(II) centers (Cd1 and Cd2) with different coordination environments. Cd1 presents a [CdO7] core composed by four Pip ligands and a MeOH molecule, while Cd2 has a [CdO6] core comprising five Pip ligands. The Cd1 metal center displays a distorted pentagonal bipyramid geometry,38 while Cd2 adopts an octahedral geometry. In this case, the Cd2 center exhibits an average twist angle of 60°, attributable to an octahedral geometry (O2−Cg1−Cg2−O1, 63.14°; O6−Cg1−Cg2−O10, 58.84°; O10−Cg1−Cg2−O2, 58.02°; average twist angle, 60°). The Cd−O bond distances range from 2.182(3) to 2.784(3) Å (Cd1) and from 2.235(4) to 2.283(3) Å (Cd2), which are similar to other reported structures with Cd(II) metal centers and carboxylate ligands39−41 (Table 5). The Cd(II) metal centers are connected through different Pip ligands with three different bridging coordination modes. In Cd1, the Pip units display the μ2-η2:η1, the μ2-η1:η1 and two equivalent μ3-η2:η1:η1 coordination modes. These Cd1 centers are related through the Pip ligands by a 2-fold axis inversion center situated between them along the polymeric chain. In the case of Cd2, the Pip ligands present three types of coordination modes: μ2-η2:η1, μ2-η1:η1, and μ3-η2:η1:η1, which are present in equivalent pairs, due to another 2-fold axis inversion center at the metal ion (Cd2).

The distorted pentagonal bipyramid geometry of Cd1 is constituted by a five-membered equatorial plane, formed by three oxygen atoms from two different Pip units presenting μ3-η2:η1:η1 coordination modes (Cd1, Cd2, Cd1) and two oxygen atoms from a Pip ligand exhibiting a μ2-η2:η1 coordination mode. The axial positions of the pentagonal bipyramid are occupied by the oxygen atom of the MeOH molecule and one carboxylate oxygen atom of a Pip unit with a μ2-η1:η1 coordination mode (Figure 8a).

In the octahedral geometry of Cd2, the four-membered equatorial plane is composed by four oxygen atoms belonging from four Pip units with two μ2-η2:η1 and two μ3-η2:η1:η1 coordination modes, while in the axial positions there are two equivalent oxygen atoms of two Pip ligands with a μ2-η1:η1 coordination mode (Figure 8a).

In this polymer, the Cd(II) atoms are linked in an alternate manner (-[Cd1−Cd1−Cd2]n-) forming a 1D chain along the a direction (Figure 8b). The linkage of the Cd1 units with Cd2 is constructed by two different bridging coordination mode of the Pip ligands (μ2-η1:η1 and a μ2-η2:η1). It is noteworthy that the Cd1 units are connected between them through a μ3-η2:η1:η1 coordination mode with which to the best of our knowledge, there is not previously reported references of Cd(II) carboxylates and few examples with Co(II)42 and Ca(II)43−45 are found in the literature.

This polymeric array presents three intramolecular interactions. The coordinated MeOH molecule promotes two of them: one strong hydrogen bond interaction34 with one carboxylate oxygen of the μ2-η1:η1 Pip unit and a C−H··· OMeOH interaction with the o-aromatic proton of the same Pip unit (Figure 9a). The remaining interaction is formed between the aromatic proton of a μ3-η2:η1:η1 Pip ligand and the carboxylate oxygen atom of the previously mentioned μ2-η1:η1 Pip unit. In addition, there is a π−π

interaction between the aromatic groups of the Pip ligands with the μ2-η2:η1 and μ3-η2:η1:η1 coordination modes (Figure 9b; Table 5).

The structure expands along the bc plane through two weak intermolecular C−H···O interactions, which form the 3D net. The dioxole ring of the Pip ligand, which presents the μ2-η1:η1 coordination mode, promotes both C−H···O interactions with two m-protons of the aromatic rings of two different Pip units: those acting as μ2-η2:η1 and a μ3-η2:η1:η1 coordination mode (Figure 10a). Moreover, the Pip ligands display a μ2-η1:η1 interact between them through a π−π interaction (Figure 10b; Table 5).

Structural Description of [Hg(Pip)2]n (4). Compound 4 belongs to the monoclinic P21/c space group. The polymeric array consists of dimeric units in which the dioxole oxygen atoms of the Pip ligands coordinate with the Hg(II) centers forming a [HgO8] core. This core is composed of two Pip units presenting a μ2-η2:η1 coordination mode and two Pip units with a μ1-η2 coordination mode, while the remaining oxygen atoms belong from the dioxole groups of neighboring Pip ligands. This metal environment generates a distorted squareantiprism geometry46 with bond angles between 51.96(9) and 165.56(10)° (Figure 11; Table 6). The coordination of the dioxole groups to the Hg(II) ions constructs an eightmembered coordination sphere, which form an aggregate of 6 dimers expanding the polymeric structure forming a 3D net (Figure 12). Seeking to compare this unusual coordination of the dioxole units, only one example with d10 metals using a dioxole containing dicarboxylate linker has been found.16

The intramolecular interactions of this compound are based on π−π stacking interactions between the aromatic rings of the Pip ligands displaying the μ2-η2:η1 and the μ1-η2 coordination modes with a value of 3.650(3) Å (Figure 13).

Hirshfeld Surface Analysis. Hirshfeld surfaces analyses of complexes 1c−4 have been performed with CrystalExplorer 2.1.47 All the surfaces have been calculated at an isovalue of 0.5 e au−3.

It is a powerful graphical tool to evaluate intra- and intermolecular interactions present in crystal structures. Owing to the aromaticity of the Pip ligand, intramolecular π−π interactions present in the polymeric complexes (2−4) have been analyzed. The curvedness surface mapping identifies planar interactions, while the 2D fingerprint plot outlines the distances between them. In the three polymers, the curvedness mapping shows planar regions through the generation of planar surfaces (Figure 14a−c). As mentioned in the structural description, curvedness mapping confirms the intramolecular π−π interactions present in compounds 2−4. In addition, the 2D fingerprint confirms that the three compounds share these planar interactions (Figure 14d−f). Compound 1c associates via hydrogen bond interaction between the coordinated water molecules and the uncoordinated carboxylate oxygen atoms. This interaction is the strongest in this system and stands out from the rest (Figure 15a). The Pip ligands generate a weaker C−H···π interaction which can be identified by a planar region in the curvedness mapping (Figure 15b).

Thermogravimetric Analysis. Simultaneous TG-DTA determinations were carried out to evaluate the thermal stability of compounds 1c, 2, and 4 (S.I: Figures S17−S19). The measurements were performed using 30.1 mg of 1c, 42.4 mg of 2, and 84.6 mg of 4. Compound 1c starts to lose the two coordinated water molecules at 90 °C (weight loss exp. 8.50%, calc. 8.4%) until 180 °C. From this temperature, the compound continues its decomposition ending at 360 °C. For compound 2, the loss of the coordinated water molecule starts at 100 °C (weight loss exp. 4.78%, calc. 4.2%) until 180 °C. It is worth to mention that there is a stable region between 180 and 210 °C presenting no mass loss. At a higher temperature, 2 starts to decompose until 370 °C. Compound 4 loses a Pip molecule between 145 and 260 °C (weight loss exp. 30.81%, calc. 31.1%). After that, there are no more thermal events.

UV−vis Spectroscopy and Photoluminescence Properties. The d orbitals' full population in Zn(II), Cd(II) and Hg(II) metal ions only allows charge transfer (CT) transitions, either between the metal and the ligand or by the ligand itself (LMCT, MLCT, and LLCT). These CTs between the $\pi-\pi^*$ orbitals are more energetic than those promoted by the d orbitals and thus fall into the UV region.48,49 The four compounds exhibit three different λmax in the range 205−293 nm as well as the free HPip ligand, and their absorption maximums are bathochromically shifted. In addition, the spectra of the complexes have a hyperchromic shift with respect to the ligand, and compound 1c presents the highest absorbance value (S.I: Figure S20).

In previous research,22 we recorded the fluorescence spectra of four Zn(II) and Cd(II) complexes with Pip and 3-phenylpyridine or 4-phenylpyridine ligands. It should be note that the aforementioned pyridine derivatives did not exhibit any fluorescence. As a continuation of this work, the photoluminescence properties of complexes 1c−4 and the free HPip ligand have been measured at 298 K in a concentration of 9.95×10^{-7} M for the HPip ligand and $\sim 1.00 \times 10^{-7}$ M for the complexes 1c−4 in MeOH solution. Their emission spectra have been depicted in Figure 16. The fluorescence emission spectra of the complexes have been carried out with an excitation wavelength of 291 nm. The fluorescence resulted in bathochromic (354−369 nm) and hyperchromic shift in emission with respect to the free ligand (346 nm). These results could be promoted by the extending of conjugation in the complexes and the more effective crystal packing in the polymeric arrays.50−52 If these results are compared with those previous reported,22 the presence of the N-auxiliary ligands did not result in a better fluorescence enhancement maybe as a consequence of the different structures and geometries. Fluorescence quantum yield (φ) is defined as the ratio of the number of photons emitted to the number of photons absorbed and describes how a fluorophore converts the excitation light into fluorescence.53 The relative fluorescence quantum yield is calculated relating the quantum yield value of the desired compound and comparing with a reference (standard).54

The quantum yields of compounds 1c−4 have been calculated using eq 1,

$$\varphi_s = \varphi_r\left(\frac{OD_{ref}}{OD_s}\right)\left(\frac{I_s}{I_{ref}}\right)\left(\frac{n_s}{n_{ref}}\right)^2 \quad (1)$$

where φref and φs, are the quantum yields of the reference and the sample, respectively. I is the area under the curve for the emission spectra, OD is the optical density (or absorbance), and n is the refractive index of the solvent. Herein, L-tyrosine has been used as the standard (φref = 0.14),55 and the values of Aref and Iref have been obtained using a 1.01 × 10−4 M solution with Milli-Q water as a solvent (nref = 1.3325)56 at r.t. The values of As and Is of HPip ligand and compounds 1c−4 have been measured in 9.95 × 10−7 M (HPip) and ∼10−7 M (1c−4) solutions using MeOH as a solvent (ns = 1.3314)57 at r.t.

The values of relative quantum yields obtained for compounds 1c−4 are 0.019 (1c), 0.033 (2), 0.053 (3), and 0.12 (4) (S.I: Table S1). These values are comparable to similar compounds with d10 metal ions reported in the literature and could be promoted by their diversity on nuclearity, coordination modes, and supramolecular structures.58,59

CONCLUSIONS

The crystal structures of 1c−4 have been elucidated, and their molecular and supramolecular interactions have been discussed. The synthesis of complexes 1c and 4 was independent of the M/L ratio. In opposite, the formation of 2 and 3 depends on this ratio and the reaction conditions (T, t). The thermal stability and the luminescent properties of the complexes have been analyzed, and their quantum yield values were calculated (4 > 3 > 2 > 1c). All the complexes showed an emission band between 350 and 375 nm. The monomeric Zn(II) complexes demonstrated a NH3−H2O exchange in solution followed by 1H NMR spectroscopy from which the final product 1c has been isolated and fully characterized. The use of the piperonylate linker in combination with d10 metal ions generated one monomeric and three polymeric structures. The diverse coordination modes of the carboxylate, ranging from μ1-η1 to μ3-η2: η1: η1, constructed different arrays. Likewise, the metal ions play an important role with a great variety of coordination numbers: 4 (1c), 6 (2), 6 and 7 (3), or 8 (4). In compound 4, this high coordination number is determined by three unusual Hg−O(dioxole) coordination bonds, which form the 3D polymeric structure. The study demonstrates that it is possible to obtain interesting structures of M(Pip)2 with different dimensionalities.

ACKNOWLEDGEMENTS

J.P. thanks CB615921 project, the CB616406 project from “FundacióLa Caixa”, and the Generalitat de Catalunya (2017/ SGR/1687). T.C. thanks the Spanish National Plan of Research MAT2015-65756R. J.A.A. thanks the Spanish National Plan of Research project CTQ2017-83632. F.S. acknowledges the PIF predoctoral fellowship from the Universitat Autònoma de Barcelona.

REFERENCES

(1) Eddaoudi, M.; Kim, J.; Rosi, N.; Vodak, D.; Wachter, J.; O'Keeffe, M.; Yaghi, O. M. Systematic Design of Pore Size and Functionality in Isoreticular MOFs and Their Application in Methane Storage. Science 2002, 295, 469−472.

(2) Ren, G. J.; Chang, Z.; Xu, J.; Hu, Z.; Liu, Y. Q.; Xu, Y. L.; Bu, X. H. Construction of a polyhedron decorated MOF with a unit network through the combination of two classic secondary building units. Chem. Commun. 2016, 52, 2079−2082.

(3) Catarineu, N. R.; Schoedel, A.; Urban, P.; Morla, M. B.; Trickett, C. A.; Yaghi, O. M. Two Principles of Reticular Chemistry Uncovered in a Metal-Organic Framework of Heterotritopic Linkers and Infinite Secondary Building Units. J. Am. Chem. Soc. 2016, 138, 10826−10829.

(4) Ke, C. H.; Lin, G. R.; Kuo, B. C.; Lee, H. M. Coordination Polymers with Bulky Bis(imidazole) and Aromatic Carboxylate Ligands: Diversity in Metal-Containing Nodes and Three-Dimensional Net Topologies. Cryst. Growth Des. 2012, 12, 3758−3765.

(5) Lu, W.; Yuan, D.; Zhao, D.; Schilling, C. I.; Plietzsch, O.; Muller, T.; Bräse, S.; Guenther, J.; Blumel, J.; Krishna, R.; Li, Z.; Zhou, H.- C. Porous Polymer Networks: Synthesis, Porosity, and Applications in Gas Storage/Separation. Chem. Mater. 2010, 22, 5964−5972.

(6) Zhou, J.; Wang, B. Emerging crystalline porous materials as a multifunctional platform for electrochemical energy storage. Chem. Soc. Rev. 2017, 46, 6927.

(7) Qiu, S.; Xue, M.; Zhu, G. Metal-organic framework membranes: from synthesis to separation application. Chem. Soc. Rev. 2014, 43, 6116−6140.

(8) Yoshioka, S.; Inokuma, Y.; Hoshino, M.; Sato, T.; Fujita, M. Absolute structure determination of compounds with axial and planar chirality using the crystalline sponge method. Chem. Sci. 2015, 6, 3765−3768.

(9) Yan, B. Lanthanide-Functionalized Metal-Organic Framework Hybrid Systems to Create Multiple Luminiscent Centers for Chemical Sensing. Acc. Chem. Res. 2017, 50, 2789−2798.

(10) Qi, Y.-J.; Wang, Y.-J.; Li, X.-X.; Zhao, D.; Sun, Y.-Q.; Zheng, S.- T. Two d10 Metal-Organic Frameworks as Low-Temperature Luminiscent Molecular Thermometers. Cryst. Growth Des. 2018, 18, 7383−7390.

(11) Zhang, D.; Xue, Z.-Z.; Pan, J.; Li, J.-H.; Wang, G.-M. Dual ligands strategy for constructing a series of d10 coordination polymers: syntheses, structures, photoluminescence and sensing properties. Cryst. Growth Des. 2018, 18, 1882−1890.

(12) Grdenic, D. The structural chemistry of mercury. Q. Rev., Chem. Soc. 1965, 19, 303−328.

(13) Tzeng, B.-C.; Huang, Y.-C.; Chen, B.-S.; Wu, W.-M.; Lee, S.-Y.; Lee, G.-H.; Peng, S.-M. Crystal-Engineering Studies of Coordination Polymers and a Molecular-Looped Complex Containing Dipyridil-Amide ligands. Inorg. Chem. 2007, 46, 186−195.

(14) Mahmoudi, G.; Morsali, A.; Zeller, M. Mercury(II) bromide/iodide coordination polymers by self-assembly of a long flexible Schiff base ligand. Solid State Sci. 2008, 10, 283−290.

(15) Ding, B.; Wu, J.; Wu, X.- X.; Huo, J.- Z.; Zhu, Z.- Z.; Liu, Y.-Y.; Shi, F.-X. Syntheses, structural diversities and characterization of a series of coordination polymers with two isomeric oxadiazol-pyridine ligands. RSC Adv. 2017, 7, 9704−9718.

(16) Dau, P. V.; Polanco, L. R.; Cohen, S. M. Dioxole functionalized metal-organic frameworks. Dalton Trans. 2013, 42, 4013.

(17) Soldevila-Sanmartín, J.; Ayllón, J. A.; Calvet, T.; Font-Bardia, M.; Pons, J. Mononuclear and binuclear copper(II) bis(1,3-benzodioxole-5-carboxylate) adducts with bulky pyridines. Polyhedron 2017, 126, 184−194.

(18) Sánchez-Férez, F.; Soldevila-Sanmartín, J.; Ayllón, J. A.; Calvet,T.; Font-Bardia, M.; Pons, J. Synthesis and characterization of three new Cu(II) paddle-wheel compounds with 1,3-benzodioxole-5-carboxylic acid. Polyhedron 2019, 164, 64−73.

(19) Soldevila-Sanmartín, J.; Ayllón, J. A.; Calvet, T.; Font-Bardia, M.; Domingo, C.; Pons, J. Synthesis, crystal structure and magnetic properties of a Cu(II) paddle-wheels complex with mixed bridges. Inorg. Chem. Commun. 2016, 71, 90−93.

(20) Sánchez-Férez, F.; Guerrero, M.; Ayllón, J. A.; Calvet, T.; Font-Bardia, M.; Planas, J. G.; Pons, J. Reactivity of homoleptic and heteroleptic core paddle wheel compounds. Inorg. Chim. Acta 2019, 487, 295−306.

(21) Sánchez-Férez, F.; Bayés, L.; Font-Bardia, M.; Pons, J. Solvent dependent formation of Cu(II) complexes based on isonicotinamide ligand. Inorg. Chim. Acta 2019, 494, 112−122.

(22) Guerrero, M.; Vázquez, S.; Ayllón, J. A.; Calvet, T.; Font-Bardia, M.; Pons, J. Zn(II) and Cd(II) Coordination Dimers Based on Mixed Benzodioxole-Carboxylate and N-Donor Ligands:

Synthesis, Characterization, Crystal Structures and Photoluminiscence Properties. ChemistrySelect 2017, 2, 632−639.

(23) Sheldrick, G. M. A Short History of SHELX. Acta Crystallogr., Sect. A: Found. Crystallogr. 2008, 64, 112−122.

(24) Macrae, C. F.; Edgington, P. R.; McCabe, P.; Pidcock, E.; Shields, G. P.; Taylor, R.; Towler, M.; van de Streek, J. Mercury: Visualization and Analysis of Crystal Structures. J. Appl. Crystallogr. 2006, 39, 453−457.

(25) Macrae, C. F.; Bruno, I. J.; Chisholm, J. A.; Edgington, P. R.; McCabe, P.; Pidcock, E.; Rodriguez-Monge, L.; Taylor, R.; van de Streek, J.; Wood, P. A. Mercury CSD 2.0 - New Features for the Visualization and Investigation of Crystal Structures. J. Appl. Crystallogr. 2008, 41, 466−470.

(26) Persistence of Vision; Persistence of Vision Pty. Ltd.: Williamstown, Victoria, Australia, 2004. http://www.povray.org/.

(27) Dolomanov, O. V.; Bourhis, L. J.; Gildea, R. J.; Howard, J. A. K; Puschmann, H. OLEX2: A complete structure solution, refinement and analysis program. J. Appl. Crystallogr. 2009, 42, 339−341.

(28) Deacon, G Relationships between the carbon-oxygen stretching frequencies of carboxylato complexes and the type of carboxylate coordination. Coord. Chem. Rev. 1980, 33, 227−250.

(29) Nakamoto, K. Infrared and Raman Spectra of Inorganic and Coordination Compounds: Part A: Theory and Applications in Inorganic Chemistry. In Wiley: Hoboken, NJ, 2009; pp 1−432.

(30) Williams, D. H.; Fleming, I. Spectroscopic Methods in Organic Chemistry; McGraw-Hill: London, UK, 1995.

(31) Abu Ali, H.; Shalash, A. M.; Akkawi, M.; Jaber, S. Synthesis, Characterization and in Vitro Biological Activity of New Zinc(II) Complexes of the Nonsteroidal Anti-Inflammatory Drug Sulindac and Nitrogen-Donor Ligands. Appl. Organomet. Chem. 2017, 31, e3772−e3786.

(32) Kennard, C. H. L.; Smith, G.; Reilly, E. J.; Stadnicka, K. M.; Oleksyn, B. J. Metal-Phenoxyalkanoic Acid Interactions. Inorg. Chim. Acta 1982, 59, 241−247.

(33) Deng, B.; Liu, Z.-D.; Liu, X.-Y.; Tan, M.-Y.; Zhu, H.-L. Diaquabis(3-Hydroxynaphthalene-2-Carboxylato-κO)Zinc(II). Acta Crystallogr., Sect. E: Struct. Rep. Online 2004, 60, m1568−m1569.

(34) Steiner, T. The Hydrogen Bond in the Solid State. Angew. Chem., Int. Ed. 2002, 41, 48−76.

(35) Morse, P. M.; Girolami, G. S. Are D0 ML6 Complexes Always Octahedral? The X-Ray Structure of Trigonal-Prismatic [Li-(Tmed)]2[ZrMe6]. J. Am. Chem. Soc. 1989, 111, 4114−4116.

(36) Friese, J. C.; Krol, A.; Puke, C.; Kirschbaum, K.; Giolando, D. M. Trigonal Prismatic vs Octahedral Coordination Geometry: Syntheses and Structural Characterization of Hexakis(Arylthiolato) Zirconate Complexes. Inorg. Chem. 2000, 39, 1496−1500.

(37) Thirumurugan, A.; Avinash, M. B.; Rao, C. N. R. 1,2-, 1,3- and 1,4-Cyclohexanedicarboxylates of Cd and Mn with Chain and Layered Structures. J. Chem. Soc., Dalton Trans. 2006, 60, 221−228.

(38) Hoffmann, R.; Beier, B. F.; Muetterties, E. L.; Rossi, A. R. Seven-Coordination. A Molecular Orbital Exploration of Structure, Stereochemistry, and Reaction Dynamics. Inorg. Chem. 1977, 16, 511−522.

(39) Stamatatos, T. C.; Katsoulakoua, E.; Nastopoulos, V.; Raptopoulou, C. P.; Manessi-Zoupa, E.; Perlepes, S. P. Cadmium Carboxylate Chemistry: Preparation, Crystal Structure, and Thermal and Spectroscopic Characterization of the One-Dimensional Polymer [Cd(O2CMe)(O2CPh)(H2O)2]n. Z. Naturforsch., B: J. Chem. Sci. 2003, 58, 1045−1054.

(40) Tahli, A.; Köc, Ü.; Elshaarawy, R.; Kautz, A.; Janiak, C. A Cadmium Anionic 1-D Coordination Polymer {[Cd(H2O)6]-[Cd2(Atr)2(M2-Btc)2(H2O)4] 2H2O}n within a 3-D Supramolecular Charge-Assisted Hydrogen-Bonded and π-Stacking Network. Crystals 2016, 6, 23.

(41) Sen, R.; Mal, D.; Brandão, P.; Ferreira, R. A. S.; Lin, Z. Cadmium-Furandicarboxylate Coordination Polymers Prepared with Different Types of Pyridyl Linkers: Synthesis, Divergent Dimensionalities, and Luminescence Study. Cryst. Growth Des. 2013, 13, 5272−5281.

(42) Gao, J.; Ye, K.; He, M.; Xiong, W.-W.; Cao, W.; Lee, Z. Y.; Wang, Y.; Wu, T.; Huo, F.; Liu, X.; Zhang, Q. Tuning metal- carboxylate coordination in crystalline metal-organic frameworks through surfactant media. J. Solid State Chem. 2013, 206, 27−31.

(43) Lamberts, K.; Englert, U. Crystal structures of coordination polymers from CaI2 and proline. Acta Crystallogr. Sect E. Crystallogr. Commun. 2015, 71, 675−680.

(44) Lamberts, K.; Porsche, S.; Hentschel, B.; Kuhlen, T.; Englert, U. An unusual linker and an unexpected node: CaCl2 dumbbells linked by proline to form square lattice networks. CrystEngComm 2014, 16, 3305−3311.

(45) Natarajan, S.; Srinivasan, B. R.; Sundar, J. K.; Ravikumar, K.; Krishnakumar, R. V.; Suresh, J. Synthesis and structural characterization of a calcium coordination polymer based on a μ3-bridging tetradentate binding mode of glycine. J. Chem. Sci. 2012, 124, 781−790.

(46) Burdett, J. K.; Hoffmann, R.; Fay, R. C. Eight-Coordination. Inorg. Chem. 1978, 17, 2553−2568.

(47) Wolff, S. K.; Grimwood, D. J.; McKinnon, J. J.; Jayatilaka, D.; Spackman, M. A. CrystalExplorer, version 2.1; University of Western, Australia: Crawley, Australia, 2007.

(48) Huheey, J. E.; Keiter, E. A.; Keiter, R. L. Inorganic Chemistry. Principles of Structure and Reactivity, 4th ed.; HarperCollins College Publishers: New York, 1993.

(49) Sutton, D. Electronic Spectra of Transition Metal Complexes; McGraw-Hill: London, UK, 1975.

(50) Que, E. L.; Domaille, D. W.; Chang, C. J. Metals in Neurobiology: Probing Their Chemistry and Biology with Molecular Imaging. Chem. Rev. 2008, 108, 1517−1549.

(51) Croitor, L.; Coropceanu, E. B.; Masunov, A. E.; Rivera-Jacquez, H. J.; Siminel, A. V.; Zelentsov; Datsko, T. Ya.; Fonari, M. S. Polymeric Luminiscent Zn(II) and Cd(II) Dicarboxylates Decorated by Oxime ligands: Tuning the Dimensionality and Adsorption Capacity. Cryst. Growth Des. 2014, 14, 3935−3948.

(52) Visscher, A.; Bachmann, S.; Schnegelsberg, C.; Teuteberg, T.; Mata, R. A.; Stalke, D. Highly selective and sensitive fluorescence detection of Zn2+ and Cd2+ ions by using an acridine sensor. Dalton Trans. 2016, 45, 5689−5699.

(53) Tarasi, S.; Azhdari Tehrani, A.; Morsali, A.; Retailleau, P. Fabrication of Amine and Imine-Functionalized Isoreticular Pillared-Layer Metal-Organic Frameworks for the Highly Selective Detection of Nitro-Aromatics. New J. Chem. 2018, 42, 14772−14778.

(54) Sommer, M. E.; Elgeti, M.; Hildebrand, P. W.; Szczepek, M.; Hofmann, K. P.; Scheerer, P. Structure-Based Biophysical Analysis of the Interaction of Rhodopsin with G Protein and Arrestin. Elsevier Inc: Amsterdam, Netherlands, 2015.

(55) Würth, C.; Grabolle, M.; Pauli, J.; Spieles, M.; Resch-Genger, U. Relative and Absolute Determination of Fluorescence Quantum Yields of Transparent Samples. Nat. Protoc. 2013, 8, 1535−1550.

(56) Chen, R. F. Fluorescence Quantum Yields of Tryptophan and Tyrosine. Anal. Lett. 1967, 1, 35−42.

(57) Hale, G. M.; Querry, M. R. Optical Constants of Water in the 200-nm to 200-nm Wavelength Region. Appl. Opt. 1973, 12, 555.

(58) El-Kashef, H. The Necessary Requirements Imposed on Polar Dielectric Laser Dye Solvents - II. Phys. B 2002, 311, 376−379.

(59) Zhang, L.; Rong, L.; Hu, G.; Jin, S.; Jia, W. G.; Liu, J.; Yuan, G. Six Zn(II) and Cd(II) Coordination Polymers Assembled from a Similar Binuclear Building Unit: Tunable Structures and Luminescence Properties. Dalton Trans. 2015, 44, 6731−6739.

Legends to figures

Scheme 1. Reaction Conditions and Coordination Modes of the Pip Ligand which Drives the Formation of Complexes 1c−4a denote the chiral C-atoms. Its origin can be from hydrolysis of L1 or the direct reaction of the intermediate reagents.

Scheme 2. Coordination Modes of the Carboxylate[a]

Figure.1 HR-ESI-MS spectra of compound 2. In detail view of (a) [Cd2(Pip)3]+ and (b) [Cd2(Pip)3(H2O)]+ fragments.

Figure.2 Molecular structure of compound 1c..

Figure.3. (a) b axis view of the supramolecular dimeric unit of compound 1c. (b) a axis view of compound 1c forming a chain along the b axis and interaction of the dimeric units..

Figure.4 (a) b axis view of compound 1c forming a chain along the a axis and interaction of the dimeric units. (b) b axis view of the zigzag chain along the c axis and interaction of the dimeric units to form it in compound 1c..

Figure.5 a axis view of the bc plane of zigzag chains in compound 1c (left). b axis view of the ac plane of zigzag chains in compound 1c (right).

Figure.6 Molecular structure of compound 2. (a) Alternate coordination modes forming the polymeric array. (b) 1D polymeric expansion along the ab direction. Only hydrogen atoms from water molecules are shown; the rest are omitted for clarity

Figure.7 (a) c axis view of the supramolecular ab plane. (b) b axis view of the supramolecular ac plane in compound 2.

Figure.8 (a) Molecular structure of compound 3. Alternate coordination modes forming the polymeric array. (b) 1D polymeric expansion along the a direction. Only hydrogen atoms from methanol molecules are shown; the rest are omitted for clarity.

Figure.9 Intramolecular interactions of compound 3 formed by (a) O−H···O and C−H···O interactions. (b) π−π interaction.

744

745 **Figure.10** Intermolecular interactions of compound 3 formed by (a) C−H···O interactions. (b) π−π
746 interaction.
747

748 **Figure.11** (Top) Molecular structure of compound 4. Hydrogen atoms are omitted for clarity. (Bottom)
749 Alternate coordination modes forming the polymeric array forming a 3D net.
750

751 **Figure.12** Dimeric units of compound 4 linked to other six dimeric units.
752

753 **Figure.13** π−π stacking interactions in compound 4. Hydrogen atoms are omitted for clarity.
754

755 **Figure.14** Hirshfeld surface curvedness mapping of Pip units in compounds (a) 2, (b) 3, and (c) 4 and
756 their corresponding fingerprint plot (d) 2, (e) 3, and (f) 4.
757

758 **Figure.15** (a) Hirshfeld surface dnorm representation and fingerprint plot of compound 1c, highlighting
759 the intermolecular interactions between the water molecules and the Pip units. (b) Hirshfeld surface
760 curvedness mapping of Pip units highlighting the C−H···π interaction.
761

762 **Figure.16** Emission spectra of complexes 1c (black line), 2 (red line), 3 (blue line), 4 (pink line), HPip
763 ligand (green line), and Ltyrosine (light blue color) excited at 291 nm in MeOH solution (9.95 × 10−7 M
764 for the HPip and ∼1.00 × 10−7 M for 1c−4 complexes) and Milli-Q water solution (1.01 × 10−4 M for
765 L-tyrosine) at r.t.
766

SCHEME 1

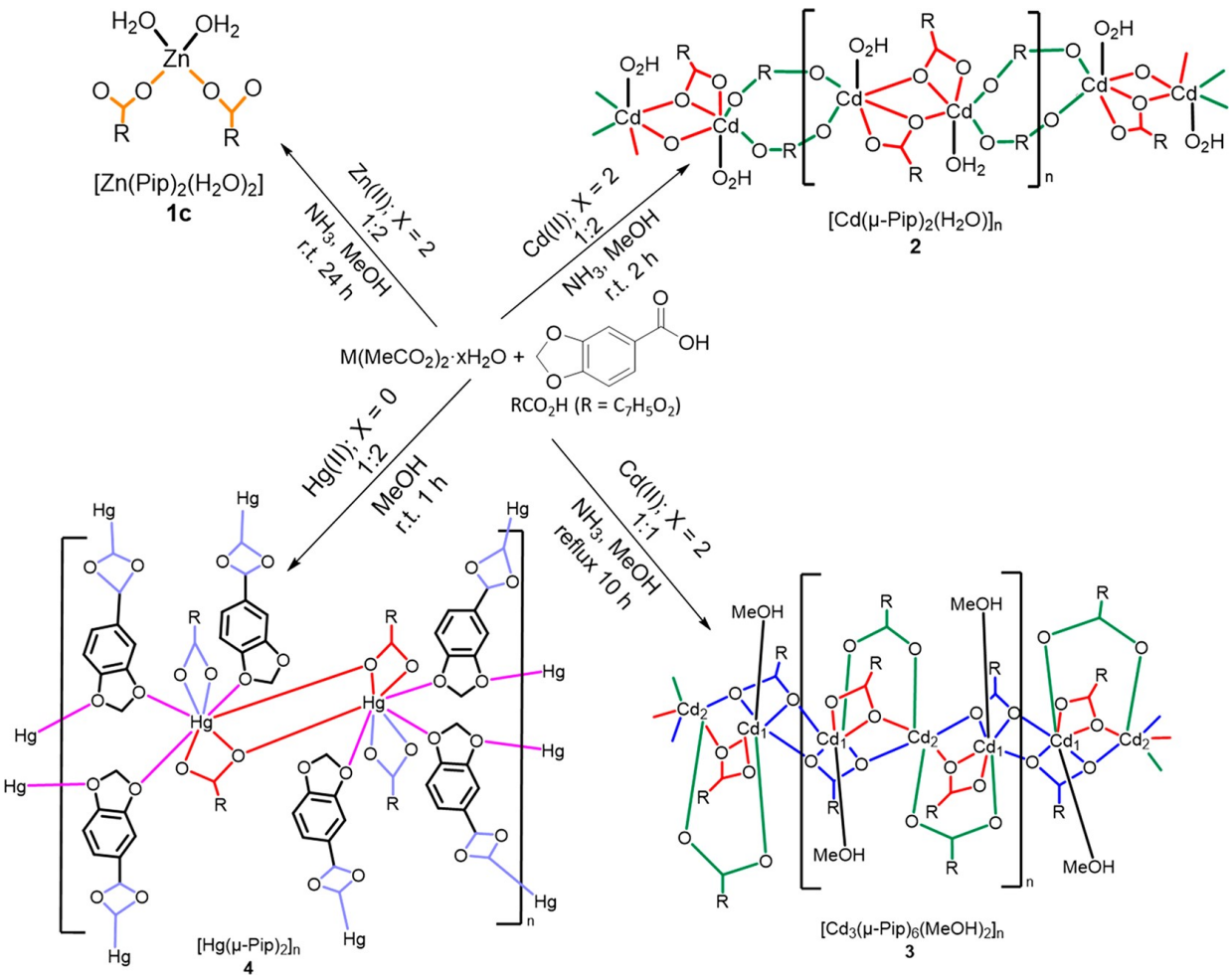
[Zn(Pip)2(H2O)2]
1c
Zn(II); X = 2
1:2
NH3, MeOH
r.t. 24 h
Cd(II); X = 2
1:2
NH3, MeOH
r.t. 2 h
[Cd(μ-Pip)2(H2O)]n
2
M(MeCO2)2·xH2O +
RCO2H (R = C7H5O2)
Hg(II); X = 0
1:2
MeOH
r.t. 1 h
Cd(II); X = 2
1:1
NH3, MeOH
reflux 10 h
[Hg(μ-Pip)2]n
4
[Cd3(μ-Pip)6(MeOH)2]n
3

FIGURE 1

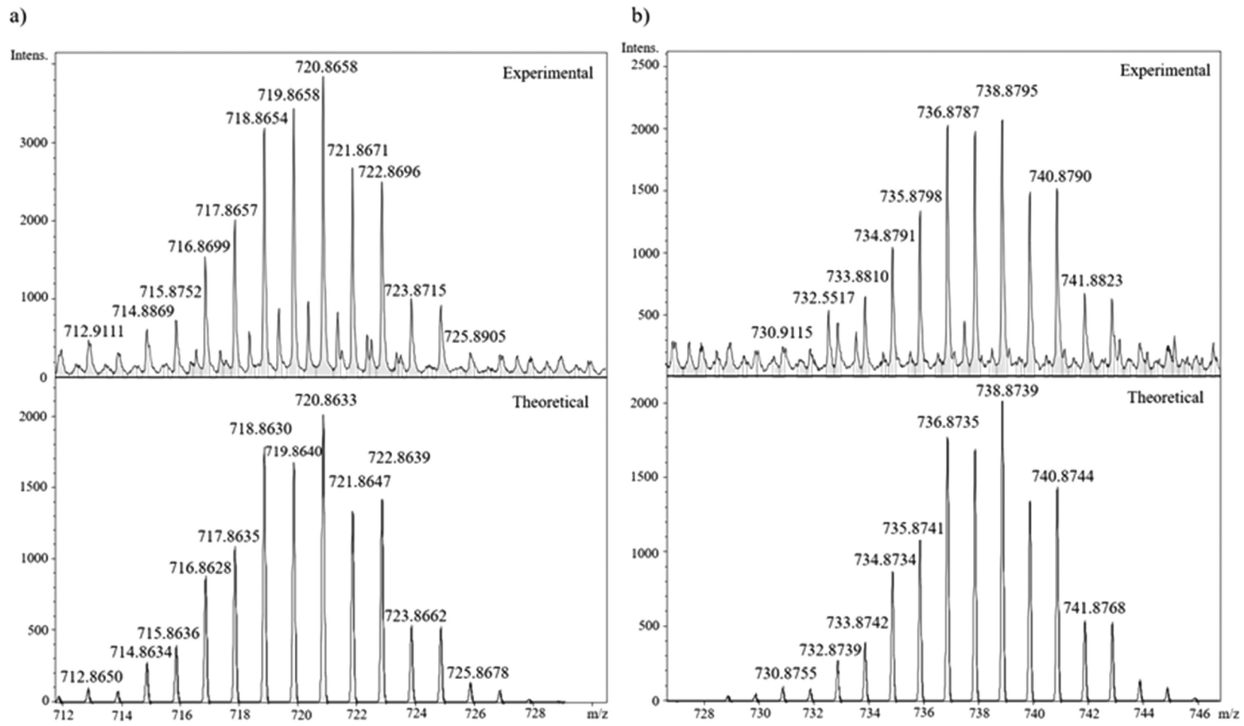
a)
Intens.
Experimental
720.8658
719.8658
718.8654
721.8671
722.8696
717.8657
716.8699
715.8752
723.8715
714.8869
712.9111
725.8905
Theoretical
720.8633
718.8630
719.8640
722.8639
721.8647
717.8635
716.8628
723.8662
715.8636
714.8634
712.8650
725.8678
712
714
716
718
720
722
724
726
728
m/z
b)
Intens.
Experimental
738.8795
736.8787
740.8790
735.8798
734.8791
733.8810
741.8823
732.5517
730.9115
Theoretical
738.8739
736.8735
740.8744
735.8741
734.8734
741.8768
733.8742
732.8739
730.8755
728
730
732
734
736
738
740
742
744
746
m/z

SCHEME 2

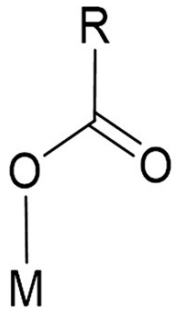

μ_1-η^1 **(1c)**

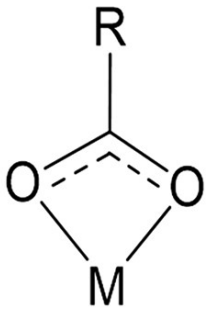

μ_1-η^2 **(4)**

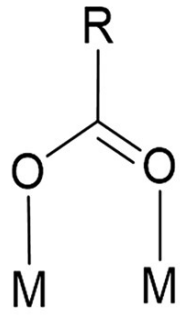

μ_2-η^1:η^1 **(2, 3)**

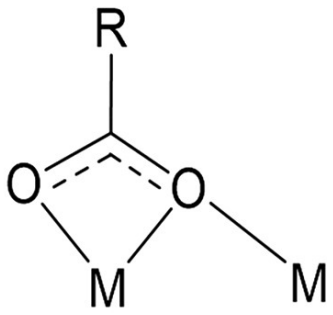

μ_2-η^2:η^1 **(2-4)**

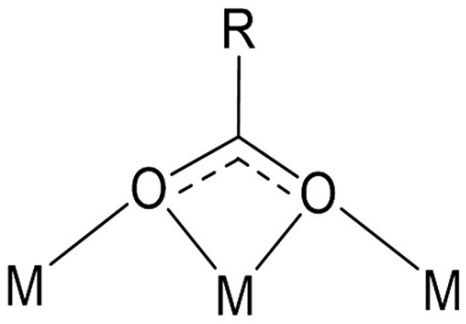

μ_3-η^2:η^1:η^1 **(3)**

FIGURE 2

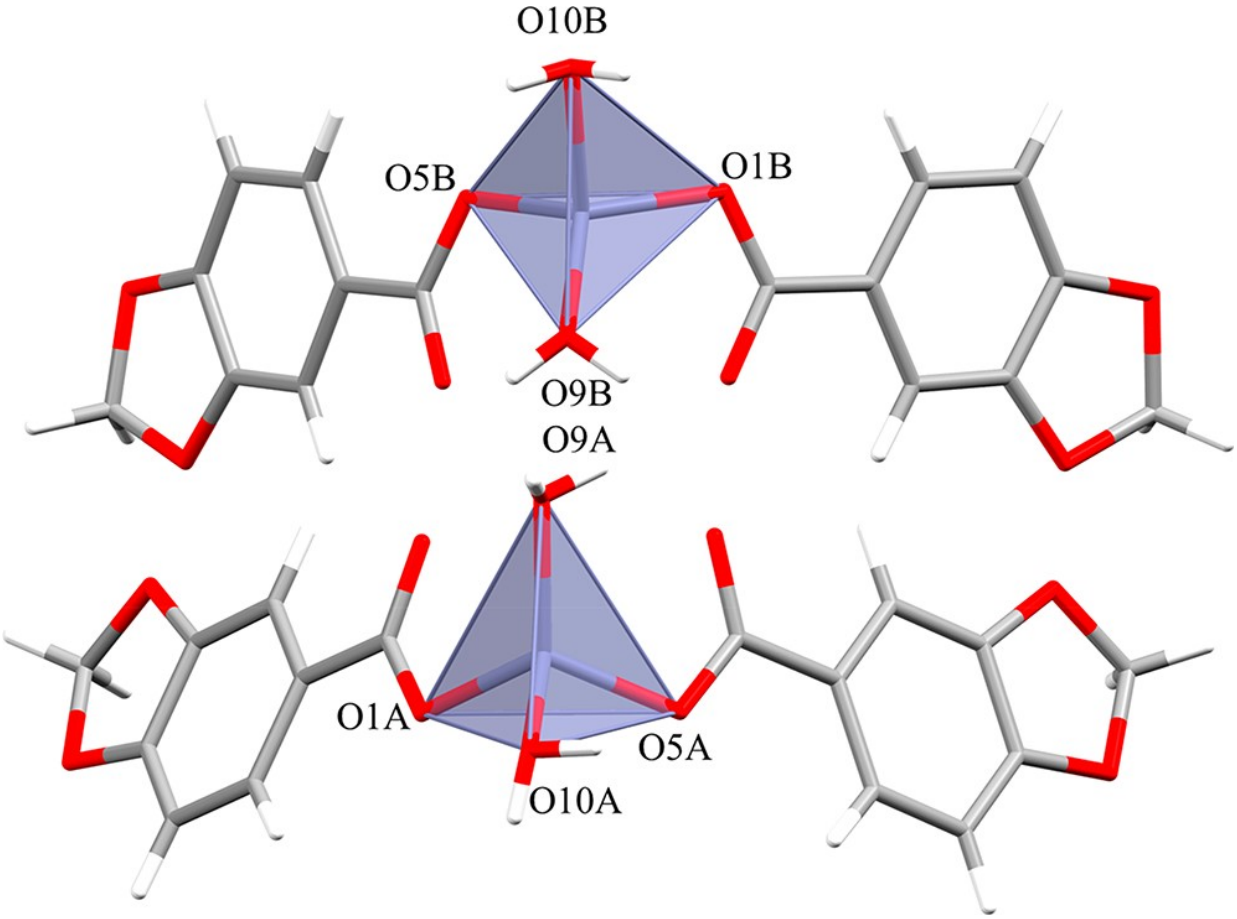

FIGURE 3

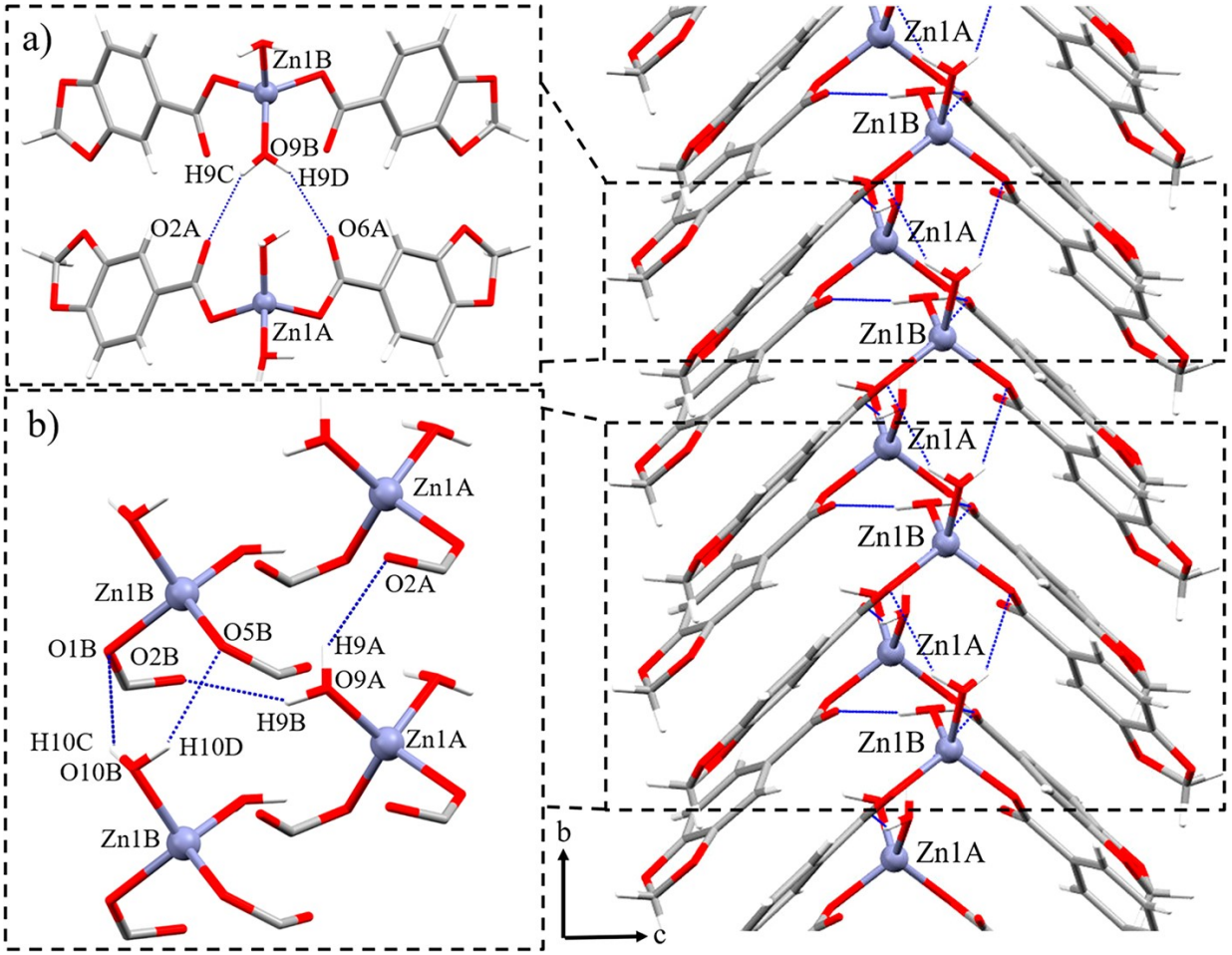
a)
Zn1B
O9B
H9C
H9D
O2A
O6A
Zn1A
b)
Zn1A
Zn1B
O2A
O1B
O2B
O5B
H9A
O9A
H9B
H10C
H10D
O10B
Zn1A
Zn1B
Zn1A
Zn1B
Zn1A
Zn1B
Zn1A
Zn1B
Zn1A
b
c

FIGURE 4

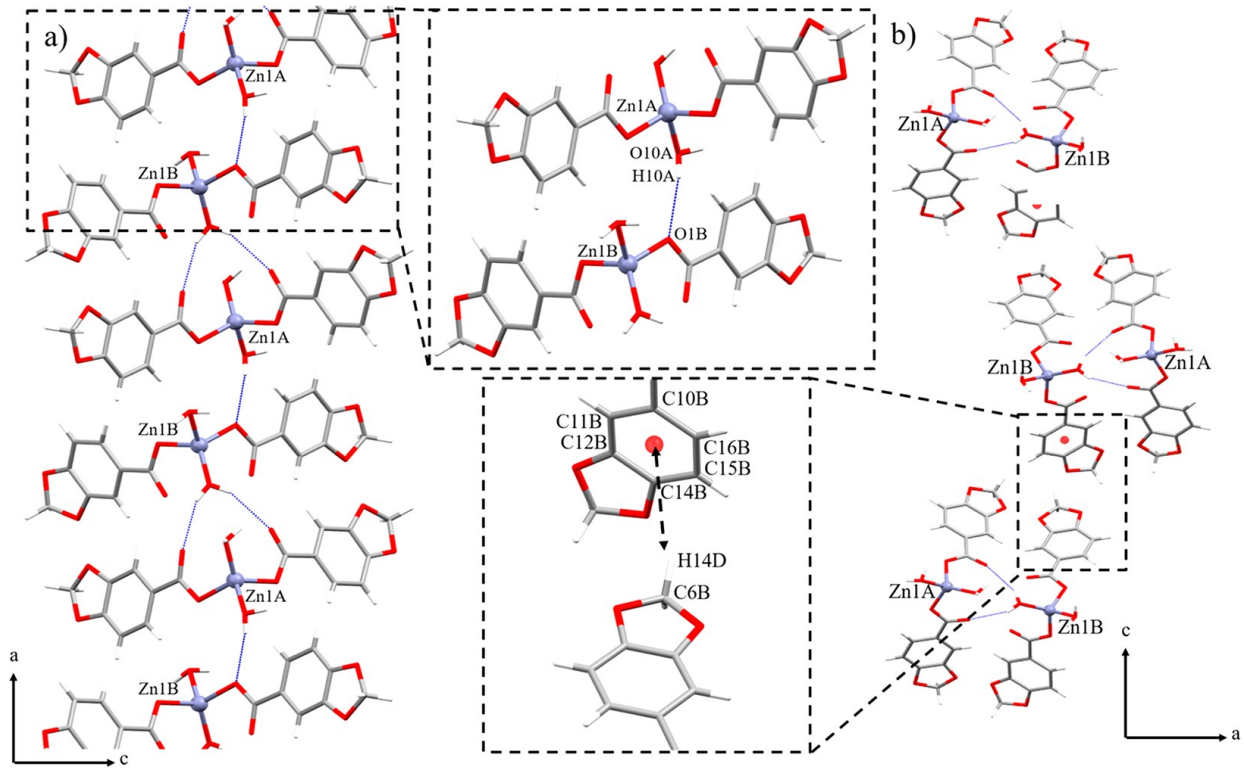
a)
Zn1A
Zn1B
Zn1A
Zn1B
Zn1A
Zn1B
O10A
H10A
O1B
C10B
C11B
C12B
C16B
C15B
C14B
H14D
C6B
b)
Zn1A
Zn1B
Zn1B
Zn1A
Zn1A
Zn1B
a
c
c
a

FIGURE 5

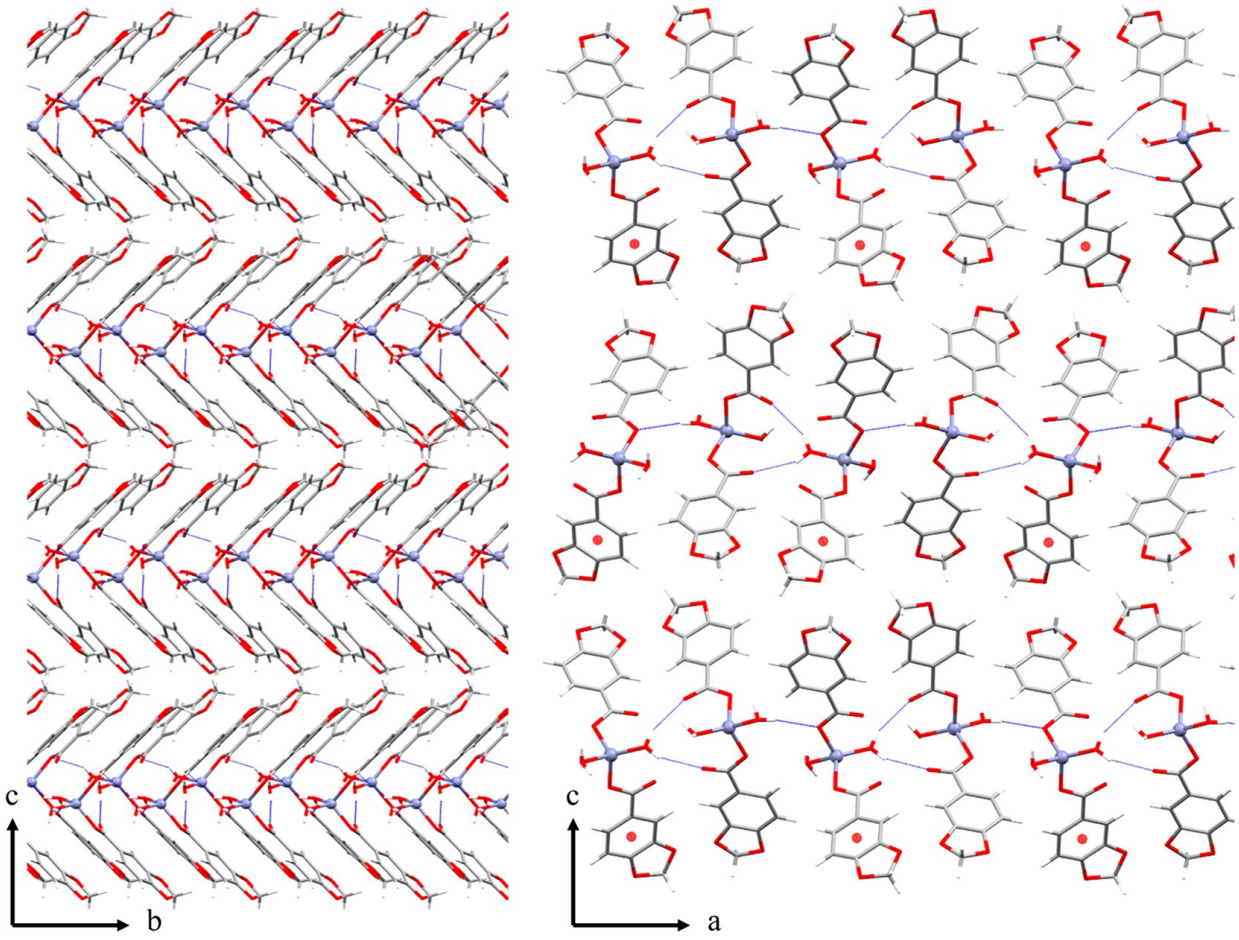

802 **FIGURE 6**

803

804

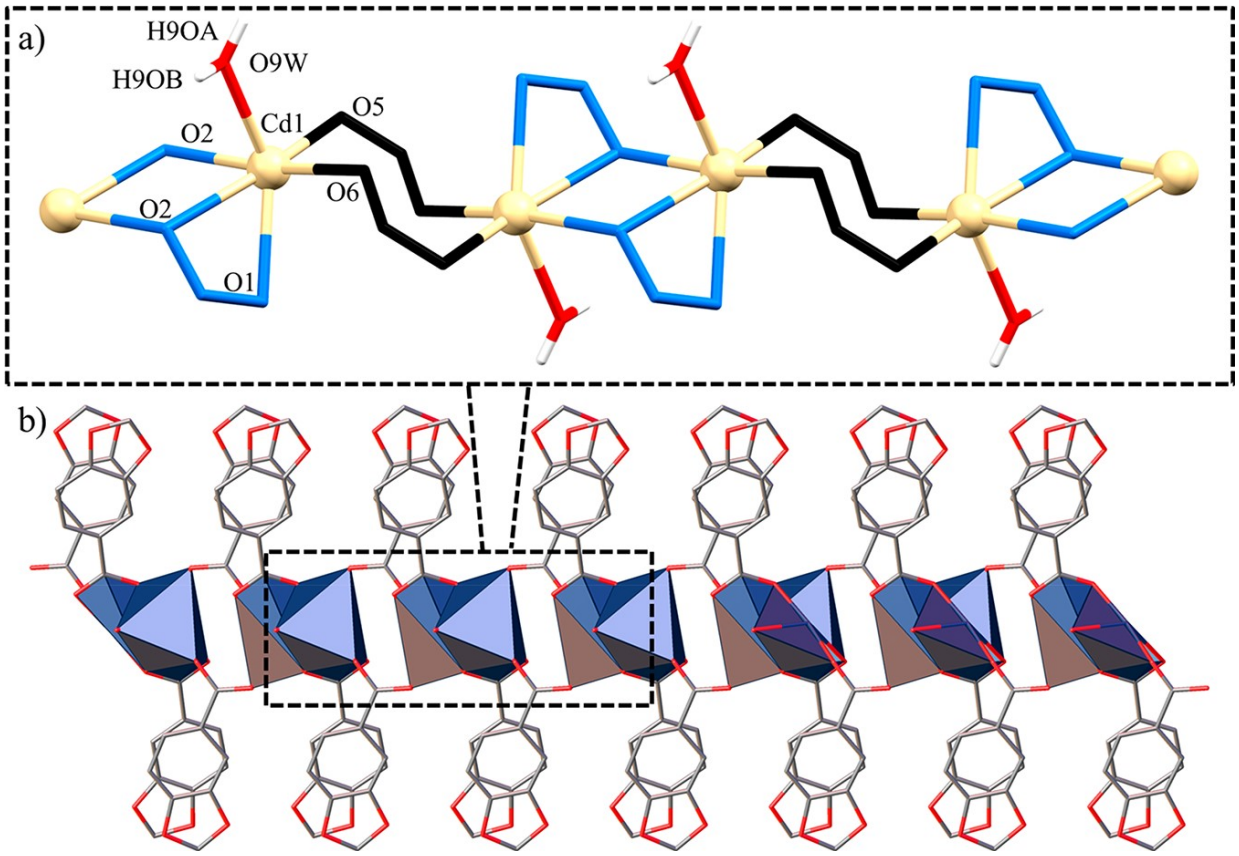

805

806

FIGURE 7

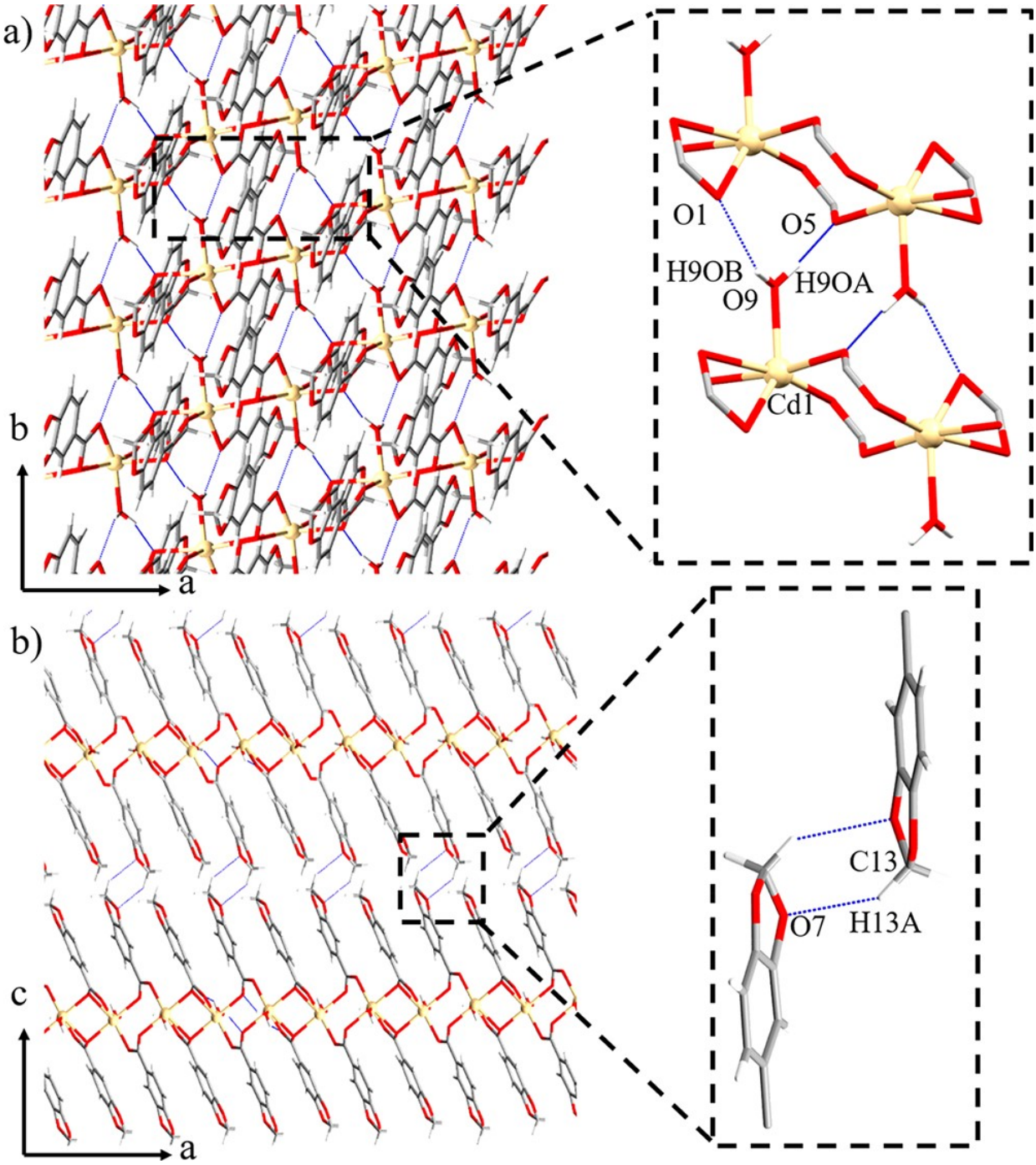

812 **FIGURE 8**

813

814

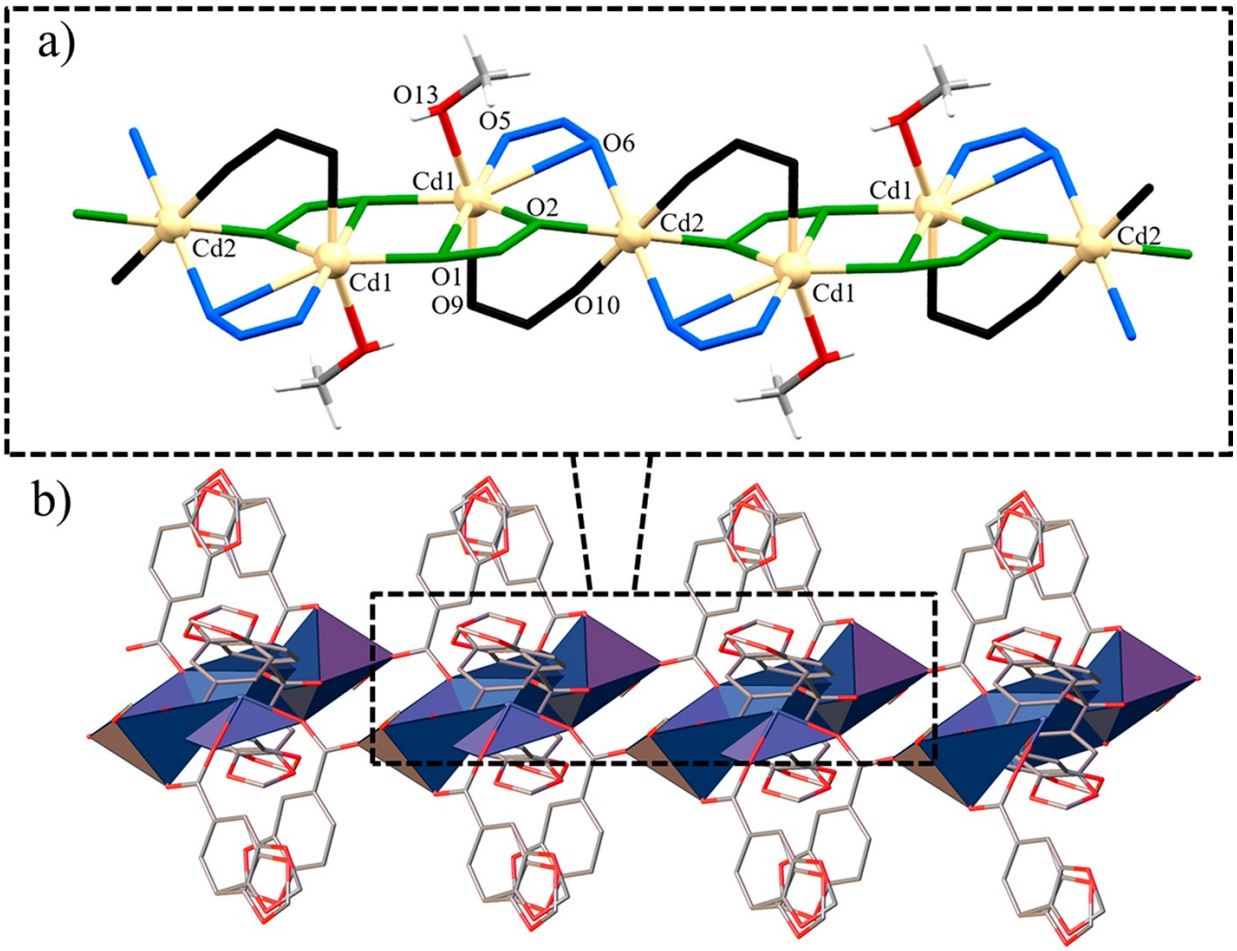

815

816

FIGURE 9

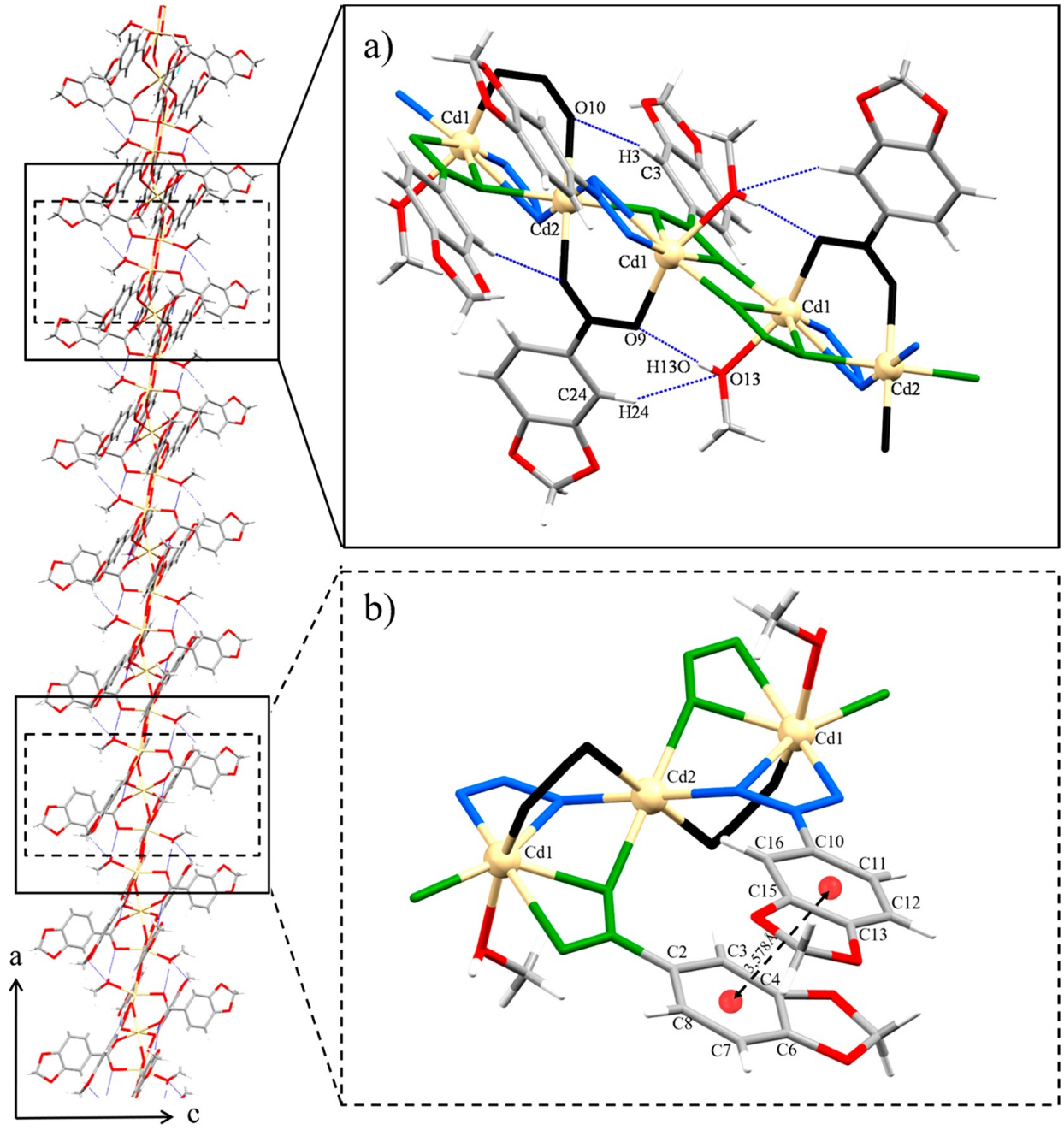
a)
Cd1
O10
H3
C3
Cd2
Cd1
Cd1
O9
H13O
O13
C24
H24
Cd2
b)
Cd1
Cd2
Cd1
C16
C10
C11
C15
C12
C13
C2
C3
3.578Å
C4
C8
C7
C6
a
c

FIGURE 10

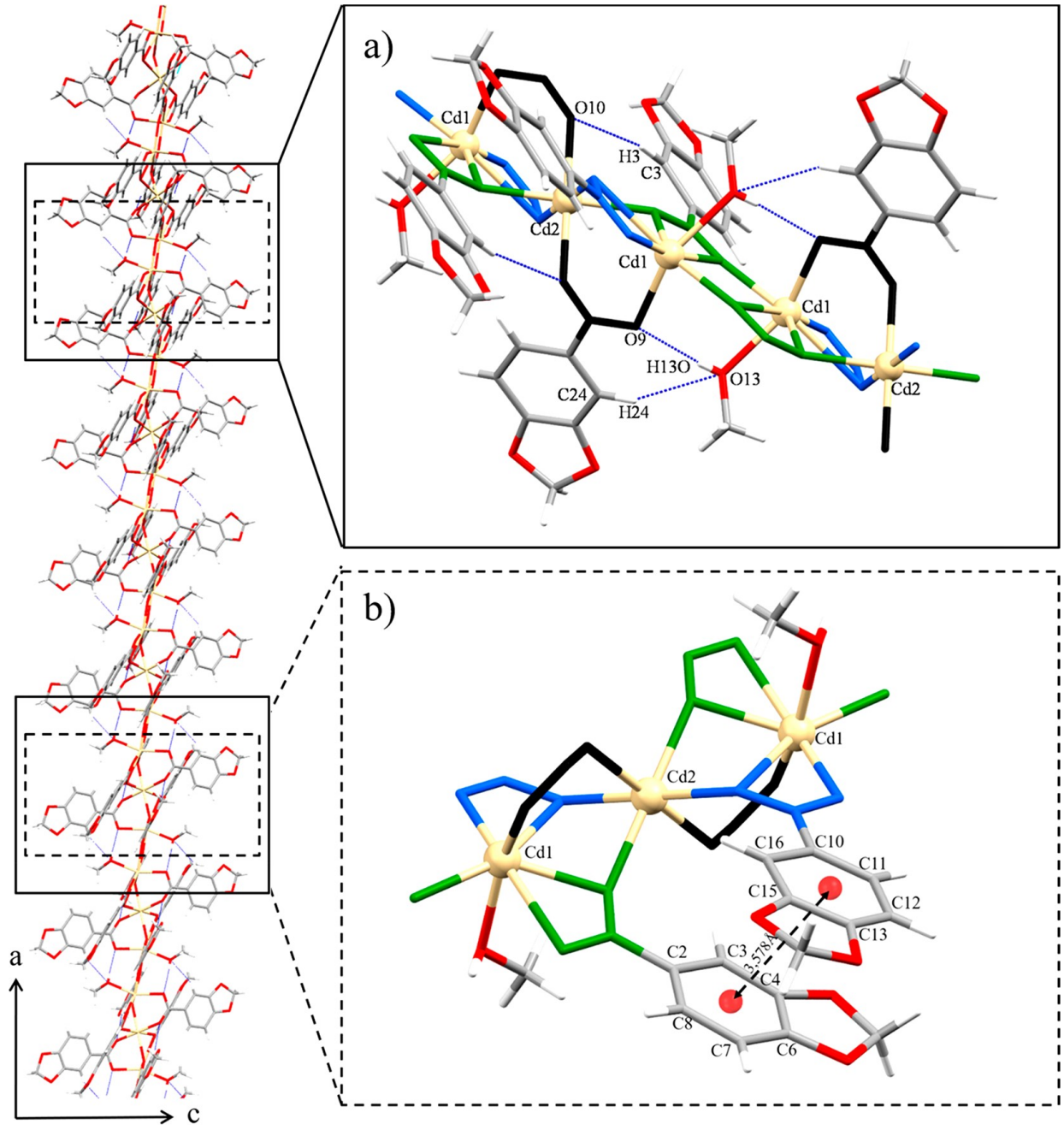
a)
Cd1
O10
H3
C3
Cd2
Cd1
Cd1
O9
H13O
O13
C24
H24
Cd2
b)
Cd1
Cd2
Cd1
C16
C10
C11
C15
C12
C13
C2
C3
3.578Å
C4
C8
C7
C6
a
c

FIGURE 11

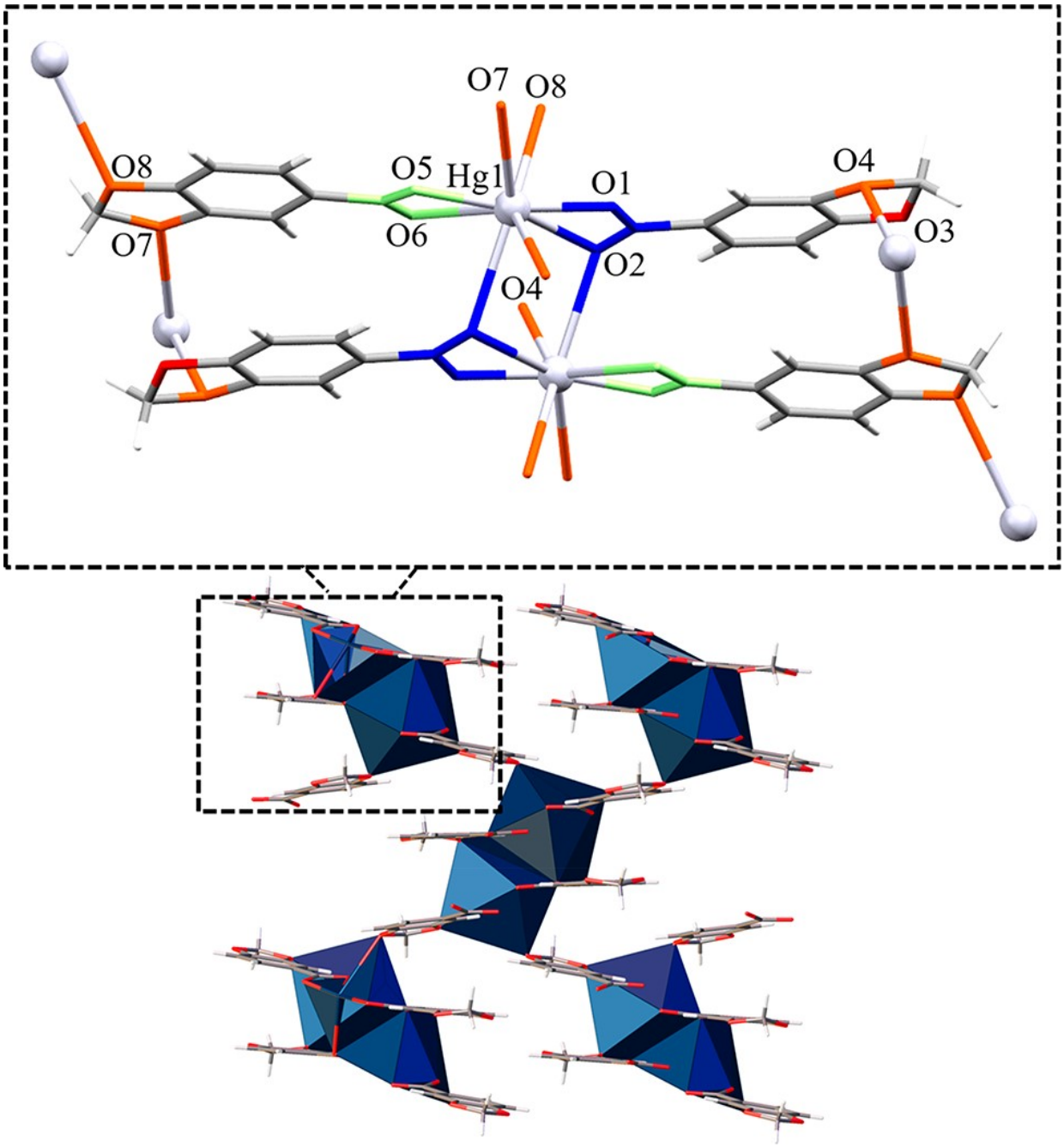

FIGURE 12

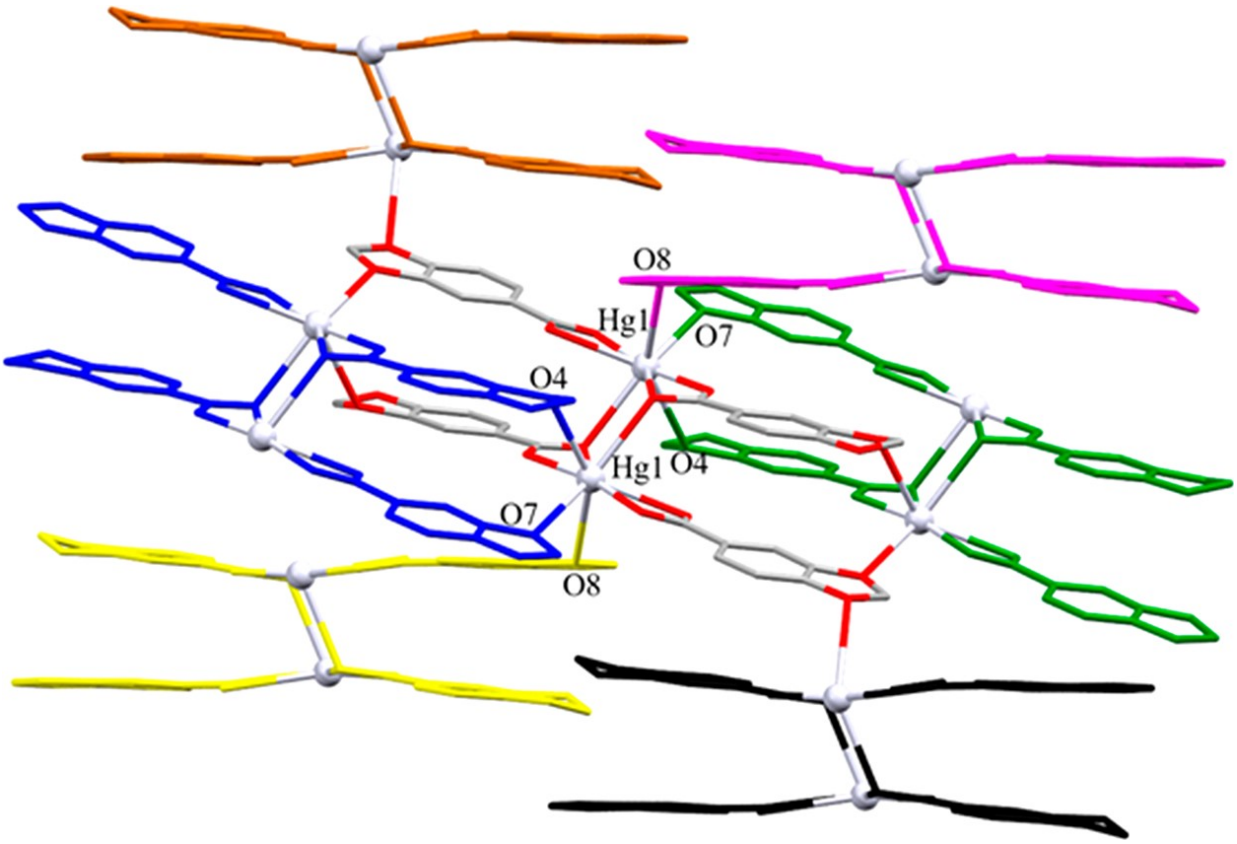

838 **FIGURE 13**

839

840

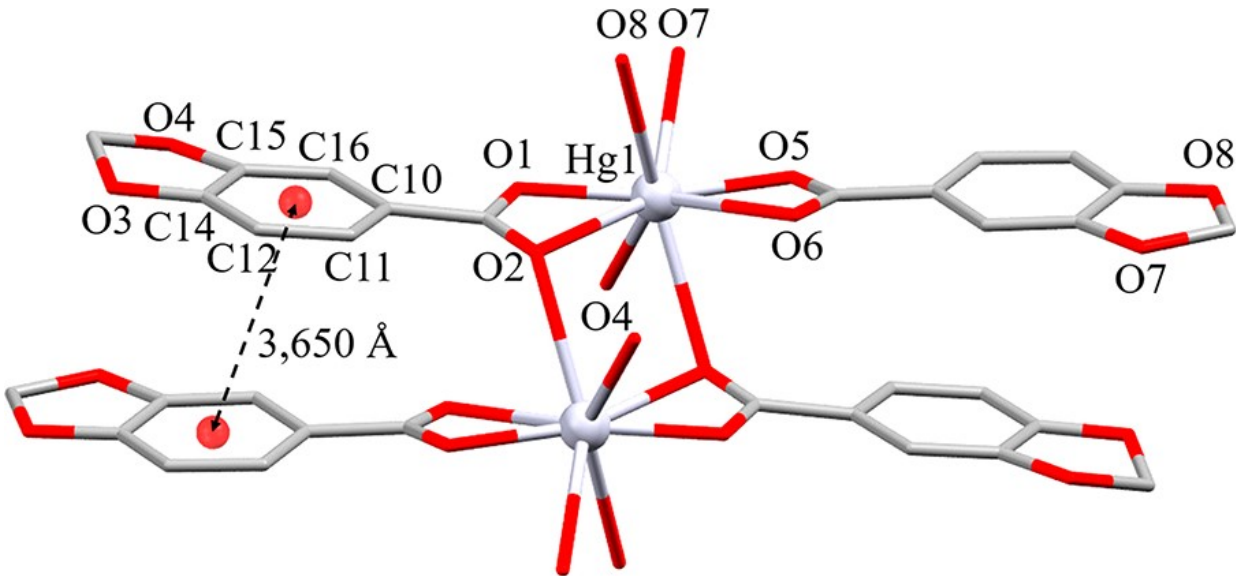

841

842

843 **FIGURE 14**

844

845

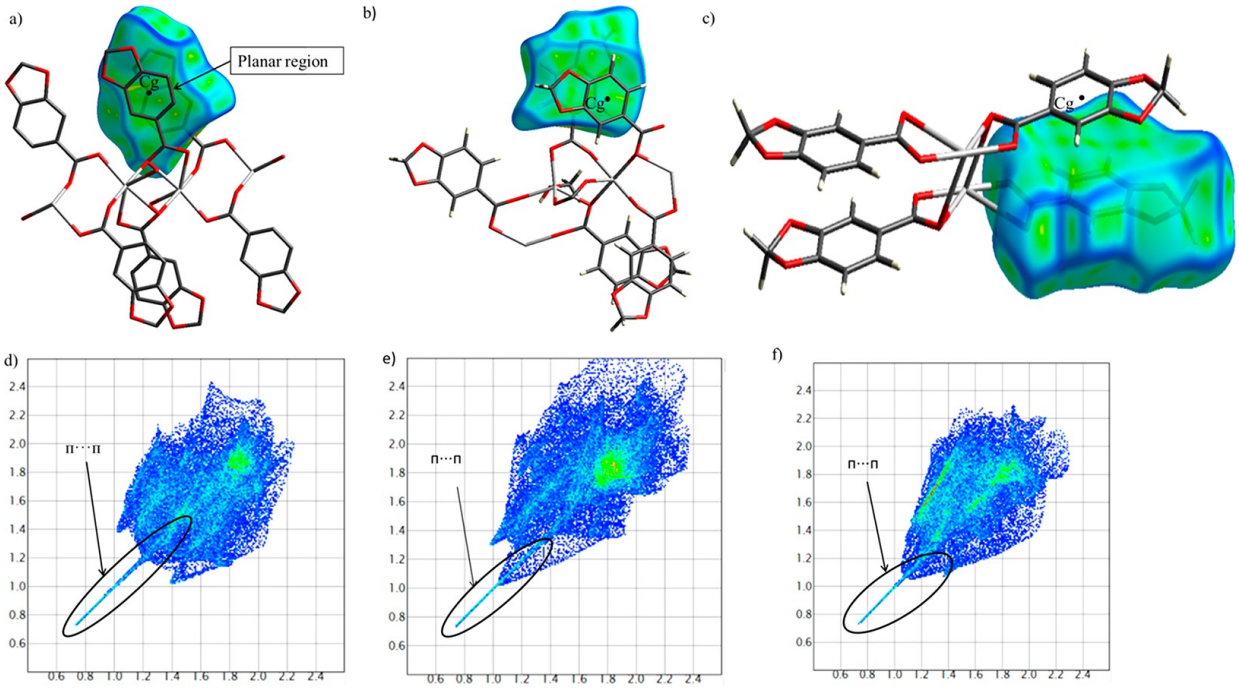

846

847

FIGURE 15

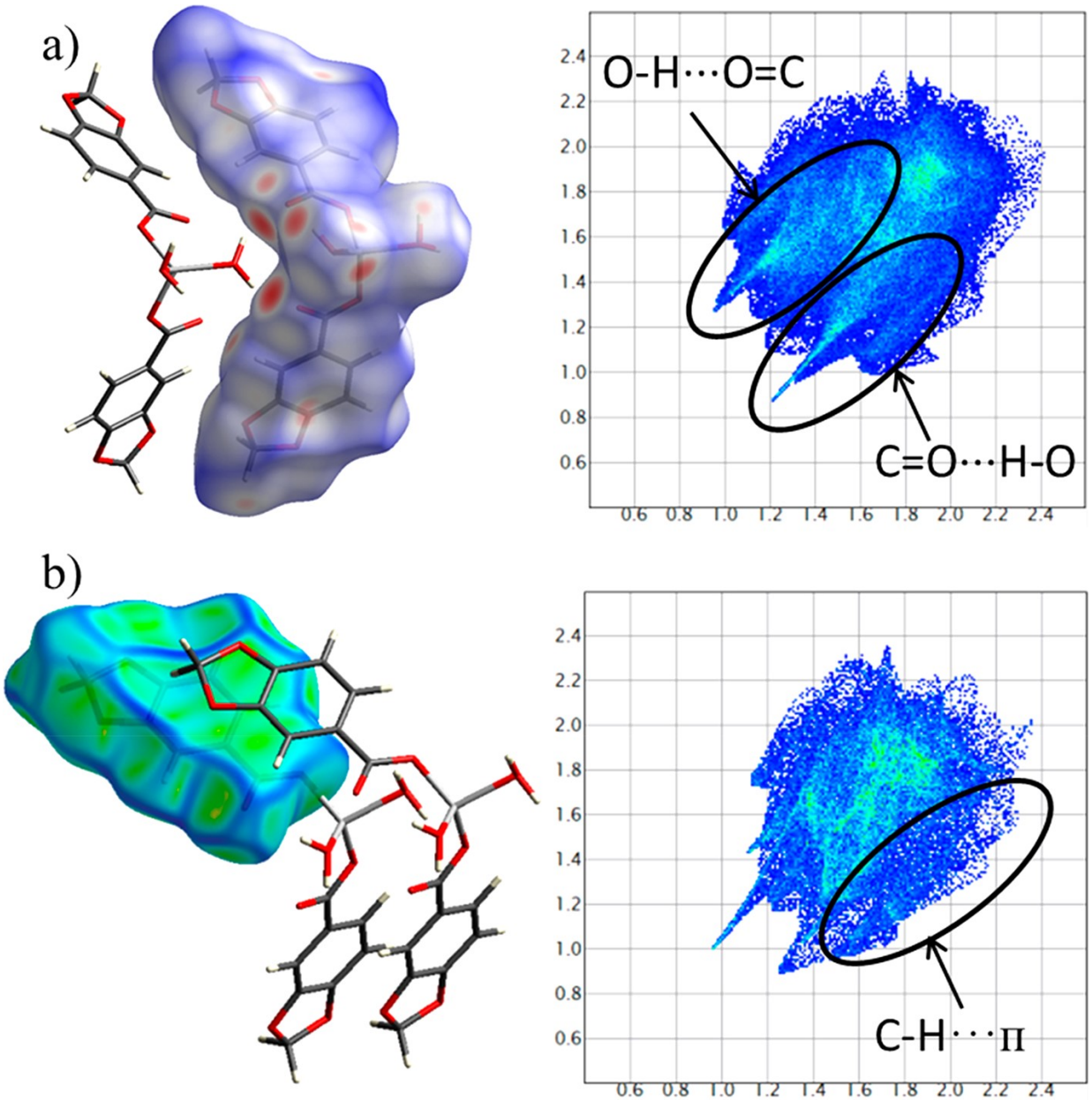

FIGURE 16

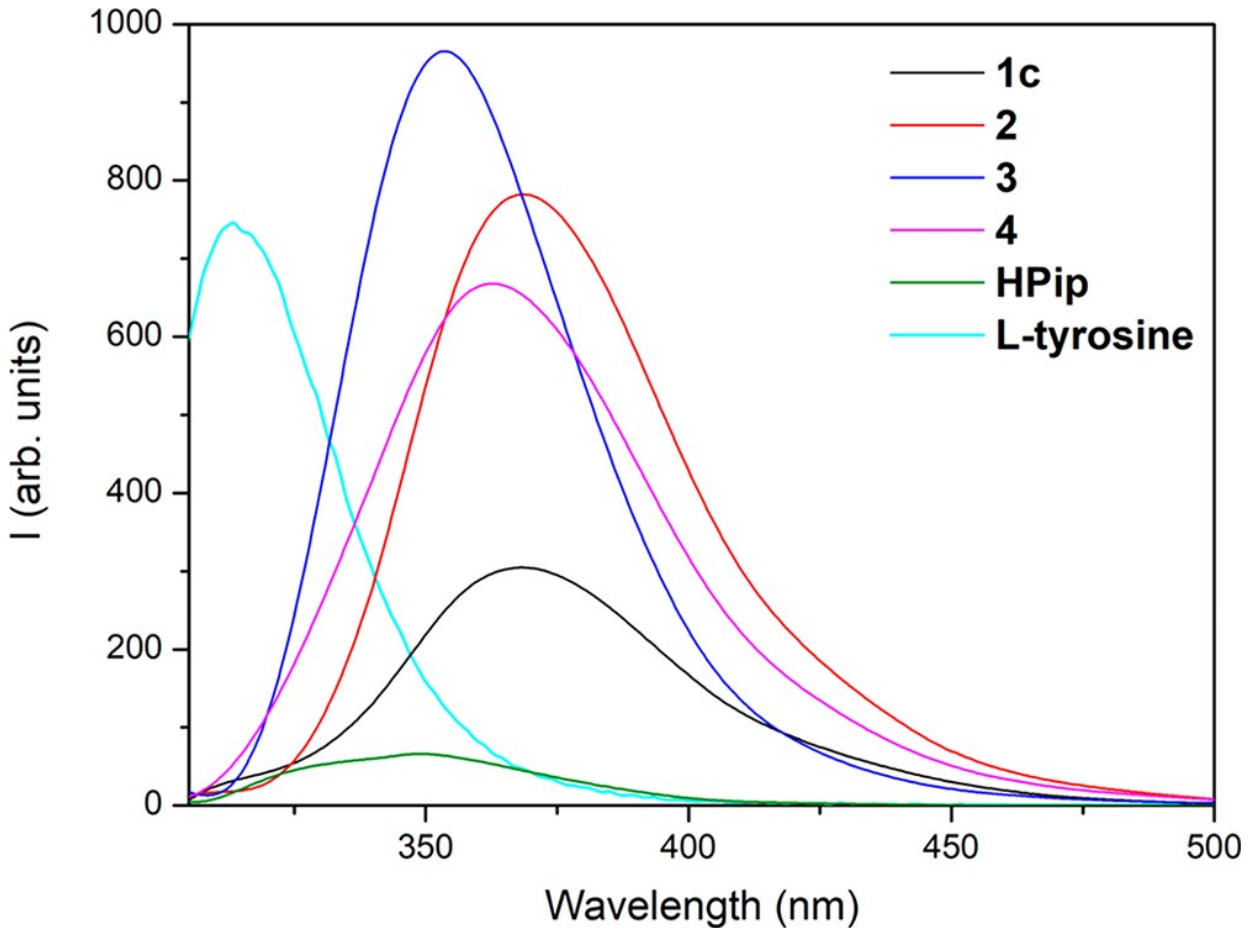
1000
800
600
400
200
0
I (arb. units)
350
400
450
500
Wavelength (nm)
1c
2
3
4
HPip
L-tyrosine

858 **Table 1.** Crystal Data and Structure Refinement for 1c−4

859

	1c	2	3	4
empirical formula	$C_{16}H_{14}O_{10}Zn$	$C_{16}H_{12}O_8Cd$	$C_{50}H_{36}O_{16}Cd_3$	$C_{16}H_{16}O_8Hg$
formula weight	431.67	460.67	1390.04	530.83
T (K)	100(2)	100(2)	100(2)	100(2)
wavelength (Å)	0.71073	0.71073	0.71073	0.71073
system, space group	orthorhombic, $Pna2_1$	monoclinic, $C2/c$	monoclinic, $P2_1/n$	monoclinic, $P2_1/c$
unit cell dimensions				
a (Å)	22.0806(19)	14.5964(14)	9.5520(5)	8.6889(18)
b (Å)	5.0458(5)	6.2617(6)	21.3082(11)	13.999(3)
c (Å)	29.021(3)	33.138(3)	12.3562(6)	12.269(3)
α (deg)	90	90	90	90
β (deg)	90	94.507(3)	102.022(2)	107.536(8)
γ (deg)	90	90	90	90
V (Å^3)	3233.4(5)	3019.45(5)	2452.0	1422.9(5)
Z	8	8	2	4
D_{calc} (mg/m^3)	1.773	2.027	1.883	2.478
μ (mm^{-1})	1.578	1.501	1.385	10.865
F(000)	1760	1824	1376	1000
crystal size (mm^{-3})	0.283 × 0.270 × 0.050	0.125 × 0.099 × 0.090	0.229 × 0.077 × 0.042	0.424 × 0.223 × 0.072
hkl ranges	$-29 \le k \le 31$	$-18 \le k \le 16$	$-13 \le k \le 11$	$-12 \le k \le 12$
	$-7 \le k \le 5$	$-7 \le k \le 7$	$-30 \le k \le 30$	$-20 \le k \le 19$
	$-41 \le l \le 39$	$-40 \le l \le 41$	$-17 \le l \le 17$	$-17 \le l \le 17$
2θ range (deg)	1.974 to 30.579	2.800 to 26.441	2.387 to 30.550	2.458 to 30.592
reflections collected/unique/ [R_{int}]	31371/9625 [R(int) = 0.0475]	23326/3061 [R(int) = 0.0478]	75108/7516 [R(int) = 0.0640]	53325/4363 [R(int) = 0.0845]
completeness to θ (%)	99.2	99.6	99.9	99.8
absorption correction	semiempirical	semiempirical	semiempirical	semiempirical
max and min transmis.	0.7461 and 0.5731	0.7454 and 0.6276	0.7461 and 0.6545	0.7461 and 0.3818
refinement method	full-matrix least-squares on F^2	full-matrix least-squares on F^2	full-matrix least-squares on F^2	full-matrix least-squares on F^2
data/restraints/parameters	9625/13/500	3061/5/230	7516/3/341	4363/0/226
goodness-of-fit on F^2	1.082	1.433	1.032	1.071
final R indices [$I > 2\sigma(I)$]	R_1 = 0.0611	R_1 = 0.0776	R_1 = 0.0543	R_1 = 0.0296
	wR_2 = 0.1631	wR_2 = 0.1790	wR_2 = 0.1317	wR_2 = 0.0506
R indices (all data)	R_1 = 0.0730	R_1 = 0.0805	R_1 = 0.0767	R_1 = 0.0469
	wR_2 = 0.1703	wR_2 = 0.1800	wR_2 = 0.1482	wR_2 = 0.0548
extinction coefficient	n/a	n/a	n/a	n/a
largest diff. peak and hole (e·Å^{-3})	2.213 and −1.562	1.463 and −3.089	2.414 and −2.206	1.626 and −1.905

860

861

862 **Table 2.** Selected Bond Lengths (Å) and Angles (deg) for Compound 1c

863

molecule A		molecule B	
	bond distances (Å)		
Zn(1A)–O(1A)	1.979(6)	Zn(1B)–O(1B)	1.973(6)
Zn(1A)–O(5A)	1.975(7)	Zn(1B)–O(5B)	1.977(6)
Zn(1A)–O(9A)	1.992(6)	Zn(1B)–O(9B)	1.998(6)
Zn(1A)–O(10A)	2.044(6)	Zn(1B)–O(10B)	2.055(6)
	bond angles (deg)		
O(1A)–Zn(1A)–O(5A)	102.8(3)	O(1B)–Zn(1B)–O(5B)	103.4(3)
O(1A)–Zn(1A)–O(9A)	120.7(3)	O(1B)–Zn(1B)–O(9B)	120.0(3)
O(1A)–Zn(1A)–O(10)	102.5(3)	O(1B)–Zn(1B)–O(10B)	101.7(3)
O(5A)–Zn(1A)–O(9A)	118.5(3)	O(5B)–Zn(1B)–O(9B)	118.7(3)
O(5A)–Zn(1A)–O(10A)	104.5(3)	O(5B)–Zn(1B)–O(10B)	105.0(3)
O(9A)–Zn(1A)–O(10A)	105.7(3)	O(9B)–Zn(1B)–O(10B)	106.0(3)

864

865

866 **Table 3**. Selected Intermolecular Interactions for Compound 1c[a]

867

	D–H···A (Å)	H–D···A (Å)	D–H (Å)	bond angle (deg)
O(9B)–H(9C)···O(2A)	2.27 (7)	3.021(9)	0.80(6)	156(6)
O(9B)–H(9D)···O(6A)	2.31 (7)	3.052(9)	0.81(5)	154(8)
O(9A)–H(9A)···O(2A)	2.41 (6)	3.060(9)	0.815(17)	137(7)
O(9A)–H(9B)···O(2B)	2.37 (7)	3.022(9)	0.82(8)	138(7)
O(10B)–H(10D)···O(5B)	2.32 (9)	3.039(9)	0.81(8)	149(8)
O(10B)–H(10C)···O(1B)	2.45 (9)	3.150(9)	0.81(7)	146(7)
O(10A)–H(10A)···O(1B)	2.51 (9)	3.145(9)	0.82(9)	136(8)
C(6b)–H(14B)···Cg(1)	3.262	4.184	0.989(6)	156

868 [a]Cg(1) = C(10B)-C(11B)-C(12B)-C(14B)-C(15B) C(16B).

869

870 **Table 4.** Selected Bond Distances (Å), Angles (deg), Torsion Angles (deg), Intra- and Intermolecular

871 Interactions (Å) for Compound 2[a]

872

bond distances (Å)			
Cd(1)–O(1)	2.371(7)	Cd(1)–O(5)	2.314(6)
Cd(1)–O(2)	2.383(7)	Cd(1)–O(6)#1	2.200(7)
Cd(1)–O(2)#2	2.393(7)	Cd(1)–O(9)	2.267(8)
Cd(1)···Cd(1)	3.705(1)	Cd(1)···Cd(1)	4.382(1)
bond angles (deg)			
O(6)#1–Cd(1)–O(9)	101.0(3)	O(5)–Cd(1)–O(2)#2	172.1(2)
O(9)–Cd(1)–O(2)	83.1(3)	O(6)#1–Cd(1)–O(2)	163.2(2)
O(1)–Cd(1)–O(2)	56.8(2)	O(6)#1–Cd(1)–O(2)#2	85.8(2)
O(6)#1–Cd(1)–O(1)	122.3(3)	O(9)–Cd(1)–O(2)#2	85.1(3)
O(5)–Cd(1)–O(2)	101.3(2)	O(1)–Cd(1)–O(2)#2	100.8(2)
O(5)–Cd(1)–O(1)	85.2(2)	O(2)–Cd(1)–O(2)#2	78.3(2)
O(9)–Cd(1)–O(5)	87.1(3)	O(9)–Cd(1)–O(1)	136.6(3)
O(6)#1–Cd(1)–O(5)	95.3(2)		
intramolecular interactions (Å)			
Cg(1)···Cg(2)	3.852(3)		
torsion angles (deg)			
O(6)–Cg(3)–Cg(4)–O(5)	56.01	O(2)–Cg(3)–Cg(4)–O(1)	46.77
O(9)–Cg(3)–Cg(4)–O(2)#2	73.07		

intermolecular interactions (Å)

D–H···A	D–H (Å)	H···A (Å)	D···A (Å)	D–H···A
O9–H9OA···O5	0.80(7)	2.00(7)	2.753(10)	155(6)
O9–H9OB···O1	0.80(8)	2.20(11)	2.677(11)	119(8)
C13–H13A···O7	0.99	2.51	3.335(13)	141

[a]#1: $-x, -y+1, -z+1$; #2: $-x+1/2, -y+3/2, -z+1$. Cg(1) = C(2) C(3) C(4) C(5) C(7) C(8). Cg(2) = C(10) C(11) C(12) C(14) C(15) C(16) [X,Y,Z]. Cg(3) = O(2) O(6) O(9). Cg(4) = O(1) O(2)#2 O(5).

873

874

Table 5. Selected Bond Distances (Å), Angles (deg), Torsion Angles (deg) and Intra- and Intermolecular Interactions (Å) for Compound 3

bond distances (Å)			
Cd(1)–O(1)	2.259(3)	Cd(1)–O(13)	2.326(4)
Cd(1)–O(1)	2.261(3)	Cd(1)···Cd(2)	3.4319(3)
Cd(1)–O(2)#1	2.285(3)	Cd(2)–O(2)#1	2.283(3)
Cd(1)–O(5)	2.182(3)	Cd(2)–O(6)	2.270(4)
Cd(1)–O(6)	2.784(3)	Cd(2)–O(10)	2.235(4)
Cd(1)–O(9)	2.262(4)	Cd(1)···Cd(1)	3.720(3)
Cd(1)···Cd(2)	3.432(3)		
bond angles (deg)			
O(1)–Cd(1)–O(2)#1	133.90(12)	O(6)#2–Cd(2)–O(2)#1	98.79(13)
O(1)–Cd(1)–O(9)	86.38(13)	O(6)#2–Cd(2)–O(6)	180.0
O(1)–Cd(1)–O(13)	79.55(14)	O(9)–Cd(1)–O(2)#1	88.87(12)
O(2)#1–Cd(2)–O(2)#3	180.0	O(9)–Cd(1)–O(13)	154.25(15)
O(2)#1–Cd(1)–O(13)	85.61(13)	O(10)–Cd(2)–O(2)#3	92.46(13)
O(5)–Cd(1)–O(1)	102.09(14)	O(10)–Cd(2)–O(6)	86.95(15)
O(5)–Cd(1)–O(2)#1	122.24(13)	O(10)–Cd(2)–O(6)#2	93.05(15)
O(5)–Cd(1)–O(9)	110.98(15)	O(10)–Cd(2)–O(2)#1	87.54(13)
O(5)–Cd(1)–O(13)	93.11(15)	O(10)#2–Cd(2)–O(2)#1	92.46(13)
O(6)–Cd(2)–O(2)#1	81.21(13)	O(10)–Cd(2)–O(10)#2	180.0

intramolecular interactions (Å)				
D–H···A	D–H (Å)	H···A (Å)	D···A (Å)	D–H···A (deg)
O(13)–H(13)···O(9)	0.65(7)	2.08(7)	2.722(6)	174(9)
C(24)–H(24)···O(13)	0.95(11)	2.51(11)	3.388(11)	155(11)
C(3)–H(3)···O(10)	0.95(6)	2.44(6)	3.377(6)	167(6)
Cg(2)···Cg(3)	3.578(4)			
torsion angles (deg)				
O(2)–Cg(1)–Cg(1)–O(6)	63.14	O(10)–Cg(1)–Cg(1)–O(2)	58.02	
O(6)–Cg(1)–Cg(1)–O(10)	58.84			
intermolecular interactions (Å)				
D–H···A	D–H (Å)	H···A (Å)	D···A (Å)	D–H···A (deg)
C(7)–H(7)···O11	0.95(9)	2.49(9)	3.403(9)	161(9)
C(12)–H(12)···O12	0.95(13)	2.39(13)	3.119(13)	133(13)
Cg(4)···Cg(4)	3.500(6)			

[a] #1 $-x+1, -y+1, -z+1$; #2 $-x, -y+1, -z+1$; #3 $x-1, y, z$. Cg(1) = O(2) O(6) O(10). Cg(2) = C(2) C(3) C(4) C(6) C(7) C(8). Cg(3) = C(10) C(11) C(12) C(13) C(15) C(16). Cg(4) = C(18) C(19) C(20) C(21) C(23) C(24).

880 **Table 6**. Selected Bond Lengths (Å) and Angles (deg) and π−π Stacking (Å) for Compound 4

881

bond distances (Å)			
Hg(1)−O(1)	2.057(3)	Hg(1)−O(5)	2.046(3)
Hg(1)−O(2)	2.753(2)	Hg(1)−O(6)	2.802(3)
Hg(1)−O(2)	2.687(2)	Hg(1)−O(7)	2.822(3)
Hg(1)−O(4)	2.855(3)	Hg(1)−O(8)	2.938(3)
Hg(1)···Hg(1)[a]	3.974(7)	Hg(1)···Hg(1)[b]	7.447(1)
Hg(1)···Hg(1)[b]	8.689(2)		
bond angles (deg)			
O(1) −Hg(1)−O(2)	52.65(9)	O(2)−Hg(1)−O(5)	82.04(9)
O(1)−Hg(1)−O(2)	108.73(9)	O(2)−Hg(1)−O(6)	75.78(8)
O(1)−Hg(1)−O(4)	75.13(9)	O(2)−Hg(1)−O(7)	130.40(8)
O(1)−Hg(1)−O(5)	165.56(10)	O(2)−Hg(1)−O(8)	138.90(7)
O(1)−Hg(1)−O(6)	138.84(9)	O(4)−Hg(1)−O(5)	102.04(9)
O(1)−Hg(1)−O(7)	92.99(9)	O(4)−Hg(1)−O(6)	136.13(8)
O(1)−Hg(1)−O(8)	79.06(9)	O(4)−Hg(1)−O(7)	79.45(8)
O(2)−Hg(1)−O(2)	86.14(8)	O(4)−Hg(1)−O(8)	150.44(7)
O(2)−Hg(1)−O(4)	107.21(8)	O(5)−Hg(1)−O(6)	51.96(9)
O(2)−Hg(1)−O(5)	139.92(9)	O(5)−Hg(1)−O(7)	72.58(9)
O(2)−Hg(1)−O(6)	88.03(8)	O(5)−Hg(1)−O(8)	99.33(9)
O(2)−Hg(1)−O(7)	139.04(8)	O(6)−Hg(1)−O(7)	115.54(8)
O(2)−Hg(1)−O(8)	66.39(7)	O(6)−Hg(1)−O(8)	73.42(7)
O(2)−Hg(1)−O(4)	64.91(8)	O(7)−Hg(1)−O(8)	87.80(7)
intramolecular interactions (Å)			
Cg(1)···Cg(2)[c]	3.650(3)		

882 [a]Intradimeric. [b]Interdimeric. [c]Cg1 = C(2) C(3) C(4) C(7) C(8). Cg2 = C(10) C(11) C(12) C(14) C(15) C(16) [1 − x, 1 − y, 1 − z].